Study on Internal Flow Condition of Contra-Rotating Small Hydro-Turbine with Spoke

By

楠　丁

Supervisor: Toru Shigemitsu

September 2018

CONTENT

Nomenclature

Q_d	: Design flow rate of the small hydro-turbine
H_d	: Design head of the small hydro-turbine
P_a	: Power assumed in a pipe of agricultural water
H_a	: Head assumed in a pipe of agricultural water
Q_a	: Flow rate assumed in a pipe of agricultural water
Q	: Flow rate in the experimental apparatus
H_{df}	: Design head of front rotor
H_{dr}	: Design head of rear rotor
N_f	: Rotation speed of front rotor
N_r	: Rotation speed of rear rotor
D	: The diameter of the casing
D_{hf}	: The hub diameter of front rotor
D_{tf}	: The tip diameter of front rotor
D_{hr}	: The hub diameter of rear rotor
D_{tr}	: The tip diameter of rear rotor
Z_f	: Blade number of front rotor
Z_r	: Blade number of rear rotor
B	: The blockage ratio of the blade
r	: Present radius of the front or rear rotor
Z	: Blade number of the front or rear rotor
t	: The thickness of front or rear blade
θ	: The setting angle of front or rear blade
t_s	: The time-step in the numerical analysis
r_c	: The radius of the casing
θ_f	: Base line angle of front rotor
θ_r	: Base line angle of rear rotor

CHAPTER 1

INTRODUCTION

In recent years, there are strong requirements to change the fossil fuel into renewable energy because of the terrible environment pollution. Renewable energy, such as hydropower, wind power, solar power, is alternative energy and can be used circularly. To suppress the greenhouse effect, the renewable energy is paid on more and more attention. Among these kinds of renewable energy, the small hydropower is not widely used now and has great potential. There are so many places that can provide the hydropower energy all over the world, and most of the small hydropower energy is not been used yet. Small hydropower facilities that generate about 100kW-1000kW have spread widely, however, it causes environmental destructions by a foundation construction and a setup of a draft tube.

On the other hand, there are a lot of places that can generate about 100W-1kW in agricultural water and a small stream. Small hydropower installations are expected to have lower environmental impacts because it will be operated near the living environment, such as agricultural water, small stream and so on. Therefore, Darrieus and gyro-type turbines, which are suitable for design specifications of a low head in agricultural water and a small river, are investigated and the performance characteristics and the optimum design parameters are discussed [1-2]. Internal flow of a spiral water turbine with wide flow passage, which has small environmental impact, is investigated [3]. Further, a small-cross flow turbine used for a small stream as an environmentally friendly pico-hydroturbine and a Savonius turbine with low cost are suggested, and the performance improvement by installation and selecting the optimum position of shield plate are reported [4-6]. Efficiency of small hydroturbine is lower than that of large one, and these small hydroturbine's common problems are easy to be out of control when there are foreign materials in the fluid media [7]. There are demands for small hydroturbine to keep high performance and wide flow passage. Therefore, we adopt the contra-rotating rotors, which can be expected to achieve high performance and enable to use low solidity rotors with wide flow passage, in order to accomplish high performance stable operation. In this study, a significant compact hydroturbine is named as a contra-rotating small hydroturbine. Final goal on this study is development of a contra-rotating small hydroturbine like electrical goods, which has portability and makes an effective use of the unused small hydropower energy resource.

Till now, some of the small hydropower energy resources in Tokushima prefecture are inspected and evaluated. The parameters, including the head, flow rate, water quality and the capacity of utilization, are investigated. As the result of the investigation and evaluation, some of the water supplying system in the farm land have great potential and can be used as the small

hydropower energy resource. Therefore, the casing of the water supplying system in the farm land is assumed as the working environment of this contra-rotating small hydroturbine. In addition, the investigation result shows that the flow rate in the casing changes in a wide range, then the contra-rotating small hydroturbine has to adjust the wide range of the flow rate, and taking advantage of this unused small hydropower energy resource is necessary.

The first step of designing this kind of contra-rotating small hydroturbine is referring to the existed design methods of the small hydroturbine, and these methods act on the designing of the low flow rate hydro-turbine which is only several liter per second [8-15]. Based on the references, we can design the rotors and blade of the contra-rotating small hydroturbine. After the designing, we can make the numerical analysis on the designing to predict the performance of the new hydroturbine, and we can make the performance experiment to prove the correction of numerical simulation.

In the previous research, because of the large loss between the front and rear rotor, we changed the geometry of the spoke from cuboid to cone. The performance and internal flow condition of this small hydro-turbine was highly improved by this modification.

In this research, a new test turbine is designed and manufactured. Compared with the original test turbine, the blade thickness and the shape of front hub of the new test turbine are changed to improve the performance and internal flow condition. On one hand, the blockage ratio of the new blade at radial direction is kept to be constant, so that the blade thickness changes during the whole radial direction. On the other hand, the length of front hub is designed to be longer than that of the original model, and the chamfer of the front hub is changed from flat plane to curved surface, so that flow direction will be changed more slowly and smoothly. The performance experiment and numerical analysis are conducted based on the new test turbine, and the differences between the original model and new model are shown and investigated [16].

To continue to optimize the geometry of the spoke, a new kind of spoke whose geometry is cylinder is designed to replace the previous cone spoke, and numerical analysis of contra-rotating small hydroturbine with cylinder spoke is conducted. The cylinder spoke is designed to increase the efficiency of this contra-rotating small hydroturbine and improve the internal flow condition between front and rear rotor. It seems that it is the cone spoke which limits the increasing of efficiency and improvement of internal flow condition [17].

Some foreign vegetable materials like leaves and grasses were put into the water to investigate the internal flow so that we are able to know the passing ability of this small hydroturbine. A high speed camera was used during the experiment and the visualization results were shown to illustrate the flowing process. The performance experiment when two pieces of small leaves were attached on the blade of front rotor was also conducted, to investigate the effect of the foreign vegetable materials on the performance of this small hydroturbine [18].

CHAPTER 2

DESIGN OF THE CONTRA-ROTATING SMALL HYDROTURBINE

The structure design is the basic step of the contra-rotating small hydroturbine. The following CFD simulation and experiment study are based on the structure design. The structure design includes the basic parameters of the contra-rotating small hydroturbine, like power, head, efficiency and rotation speed. Besides, it also includes the design of the blade, the design of the rotor and the stacking of the blade. To improve the performance of the contra-rotating small hydro-turbine, we make modifications on the blade and front rotor. We also change the geometry of the spoke from cone to cylinder, to improve the flow condition near the spoke. The CFD simulation about the cylinder spoke is conducted and flow condition near the spoke is proved to be improved by the numerical result.

2.1 The working environment and parameters

The working environment of the contra-rotating small hydroturbine is preferred to be into the water pipe in the farm land. The energy in the water pipe is planned to be used by the contra-rotating small hydroturbine. The basic parameters of the working environment are as below: the power is about 10-100W, the head is about 1-4m, the flow rate of the water is about 2-10L/s. The working environment and water pipe in the farm land are shown in Figure 2-1.

Figure 2-1 The working environment of the contra-rotating small hydroturbine

Based on the above working environment, the basic parameters of the contra-rotating small

hydroturbine, like power P[kW], flow rate Q_d[m^3/s], head H[m], rotation speed N[rpm], are decided. The design heads of each front and rear rotor are the same as $H_{df}=H_{dr}$=1.3m and rotation speeds of each front and rear rotor of the test turbine are $N_f=N_r$=2300r/min considering a characteristic of a small generator which can produce about 10-100W.

The design power of the contra-rotating small hydroturbine is 80W, the design head of the contra-rotating small hydroturbine is 2.6m, the design flow rate of the contra-rotating small hydroturbine is 4.825L/s, the design rotation speed is 2300r/min. The design head of the front rotor is 1.3m, the design head of the rear rotor is 1.3m, the design power of the front rotor is 40W, the design power of the rear rotor is 40W. The design rotation speed of the front rotor and rear rotor is 2300r/min.

2.2 The design of the structure

2.2.1 The design of the blade

The blade is the key component of the turbo-machinery, when the turbo-machinery is working, the blade receives the impact of the water, and then the torque is generated and the torque acts on the rotor. Therefore, the design of the blade will have important effect to the whole rotor. When we design the blade, firstly we will consider the shape of the blade, and then we will force on the airfoil profile. We choose NACA6512 as the airfoil profile of the blade. The name role of the NACA series blade is shown in Figure 2-2:

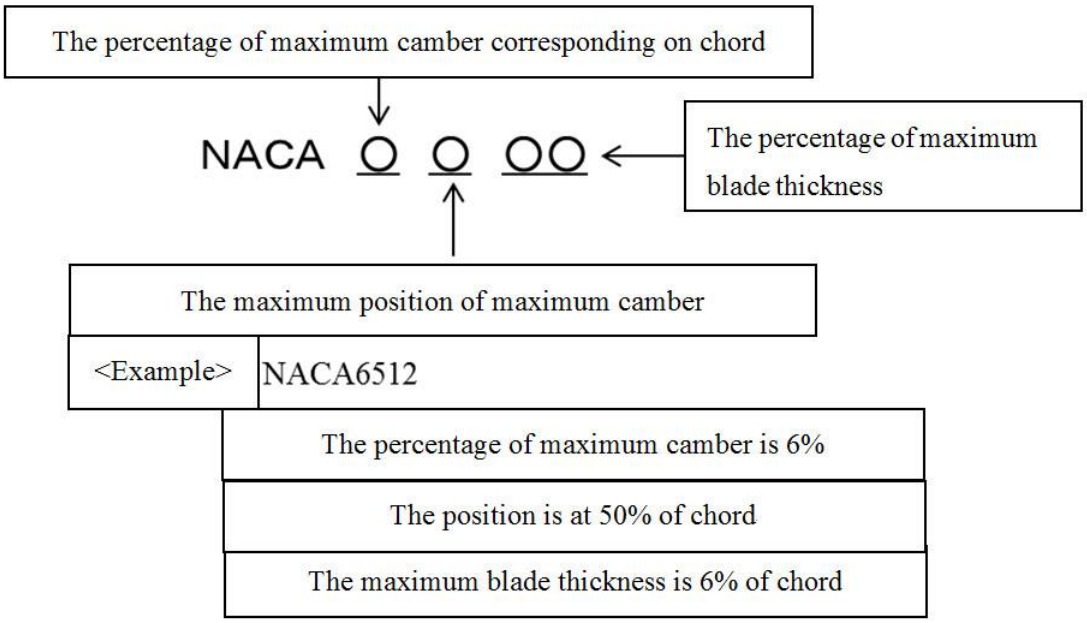

Figure 2-2 The name role of the NACA series blade

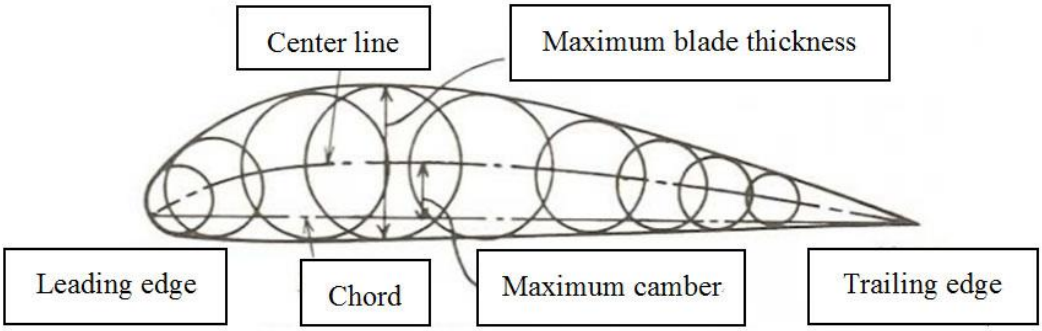

Figure 2-3 The parameters of the blade

The parameters of the blade are shown in Figure 2-3. The parameters include the center line, the maximum the blade thickness, the leading edge, the chord, the maximum camber, and the trailing edge.

The blade profile can be calculated. The coordinate of the points on the upper half part of the blade is calculated as the following equation:

$$\begin{cases} x_u = x - y_t \sin\theta \\ y_u = y_c + y_t \cos\theta \end{cases} \tag{2-1}$$

The coordinate of the points on the lower half part of the blade is calculated as the following equation:

$$\begin{cases} x_l = x + y_t \sin\theta \\ y_l = y_c - y_t \cos\theta \end{cases} \tag{2-2}$$

The coordinate of the points on the center line of the blade is calculated as the following equation:

$$y_c = \begin{cases} \dfrac{m}{p^2}(2px - x^2) & ; 0 \le x \le p \\ \dfrac{m}{(1-p)^2}\left\{(1-2p) + 2px - x^2)\right\} & ; \ p \le x \le 1 \end{cases} \tag{2-3}$$

The angle θ is calculated as the following equation:

$$\theta = \frac{dy_c}{dx} = \begin{cases} \dfrac{m}{p^2}(2p - 2x) & ; 0 \le x \le p \\ \dfrac{m}{(1-p)^2}(2p - 2x) & ; \ p \le x \le 1 \end{cases} \tag{2-4}$$

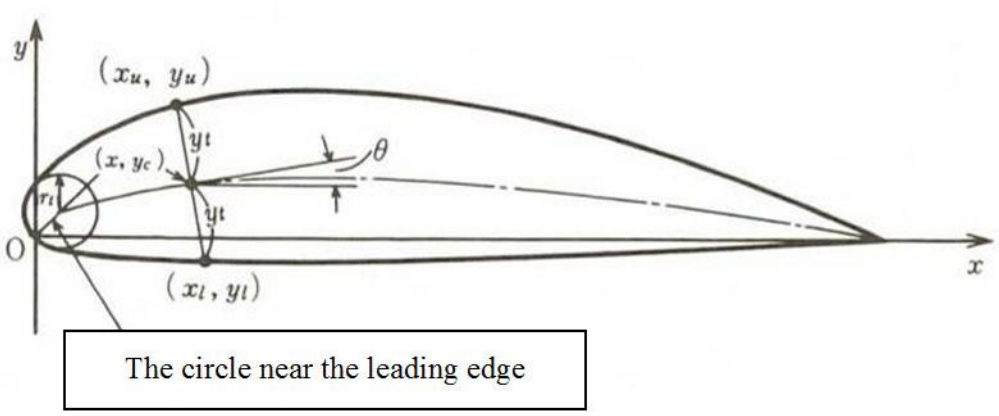

Figure 2-4 The drawing process of the blade profile

The blade thickness of the contra-rotating small hydroturbine is calculated as the following equation:

$$y_c = \frac{t}{0.20}(0.29690\sqrt{x} - 0.12600x - 0.35160x^2 + 0.28430x^3 - 0.10150x^4) \quad (2\text{-}5)$$

Then we can obtain the airfoil profile of the contra-rotating small hydroturbine. The drawing process is shown in Figure 2-4.

2.2.2 The design of the rotor

The next working is design of the rotor. The blade is connected with rotor, and the size of the rotor is very important for the whole contra-rotating small hydro-turbine.

The first step of designing the rotor is to calculate the specific speed N_S. According to the definition of the N_S, it can be calculated by the rotation speed, the power and the head. The equation of calculating the N_S is shown as following equation:

$$N_S = N \times \frac{P^{\frac{1}{2}}}{H^{\frac{5}{4}}} \quad (2\text{-}6)$$

Then we can obtain the specific speed N_S. This parameter is very important and it is often used in the following calculating process.

The second step is designing the rotor is deciding the circumferential velocity coefficient K_u and the hub diameter coefficient K_b. These two parameters can be referred by the graph. This graph can help us to know the velocity coefficient K_u and the hub diameter coefficient K_b by the specific speed N_S. The graph is shown in Figure 2-5.

We can also calculate the circumferential velocity u, the diameter of the whole rotor D_o, and the diameter of the hub D_b, they are calculated as following:

$$u = K_u\sqrt{2gH} \quad (2\text{-}7)$$

$$\because u = \frac{\pi D_O N}{60} \tag{2-8}$$

$$\therefore D_O = \frac{60u}{\pi N} \tag{2-9}$$

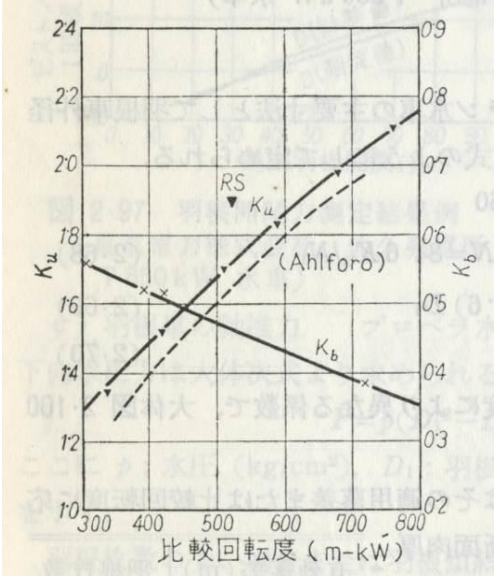

Figure 2-5 The graph of K_u and K_b

Therefore, we can obtain the diameter of the whole rotor D_o, and the diameter of the hub D_b, they are as below:

$$D_O = \frac{60}{\pi N} K_u \sqrt{2gH} \tag{2-10}$$

$$D_b = K_b D_O \tag{2-11}$$

The third step is deciding the blade number of front rotor and rear rotor. We can decide the blade number based on the tradition design experiences. Based on the tradition design experiences of axial hydro-turbine, the blade number can be decided in Table 2-1:

Table 2-1 Tradition design experiences of blade number

Head [m]	Blade number
5-15	4
10-30	5
20-40	6
30-50	7
50-80	8

Based on the tradition design experiences of axial hydro-turbine, we decide that the blade number of front rotor is four. Considering that the blade number of the front rotor and rear rotor should be co-prime, we decide that the blade number of front rotor is four and the blade number of rear rotor is three.

The fourth step is calculating the average axial velocity V_m. When we calculate this average axial velocity, we assume that the flow section is circular ring. Considering the effect of the blade, we will multiply a coefficient K_m, and this K_m is ranged from 0.75 to 0.9. How to choose this K_m is based on the experiences and the using environment. The equation of calculating the average axial velocity is shown as below:

$$Q_d = K_m \times S \times V_m \tag{2-12}$$

Because the flow section is circular ring, the area of the circular ring can be calculated as the following equation:

$$S = \pi\left(\frac{D_O}{2}\right)^2 - \pi\left(\frac{D_b}{2}\right)^2 \tag{2-13}$$

Based on the equation of (2-12) and (2-13), we can obtain the equation of calculating the average axial velocity, it is shown as below:

$$V_m = \frac{4Q_d}{\pi\left(D_O{}^2 - D_b{}^2\right) \times K_m} \tag{2-14}$$

The fifth step is calculating the average inlet angle of the water.

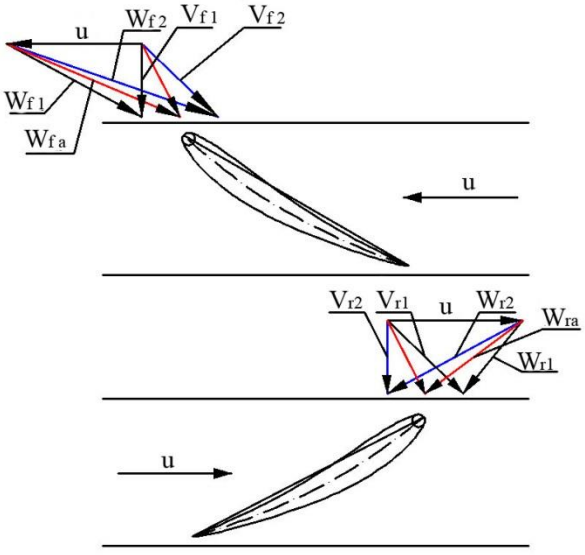

Figure 2-6 Flow schematic diagram of contra-rotating rotor

The contra-rotating rotors consist of front rotor and rear rotor, and the front rotor and rear rotate in contrary direction. The flow direction of the water will be changed when it flow into the front blade. Then the turbulent kinetic energy behind the front rotor can be taken advantaged by the rear rotor. After that, the water flow into the rear rotor, and the flow direction is changed into the original direction, and finally flow to the downstream of the whole contra-rotating rotor. The flow schematic diagram of contra-rotating rotor is shown in Figure 2-6.

Therefore, the front average inlet angle of the water β_{fa} can be calculated as below:

$$\beta_{fa} = \tan^{-1}\left(\frac{V_m}{u + \frac{V_{fu2}}{2}}\right) \tag{2-15}$$

According to the energy transforming theory of fluid machinery, the calculating equation of the theory head is shown as below:

$$H_{th} = \eta_h \times H \tag{2-16}$$

And according to the Euler equations of the fluid machinery, we can obtain the following equation:

$$H_{th} = \frac{u}{g}\left(V_{fu1} - V_{fu2}\right) \tag{2-17}$$

$$H_{th} = \frac{u}{g} \times V_{fu2} \tag{2-18}$$

$$V_{fu2} = \frac{\eta_h \times H \times g}{u} \tag{2-19}$$

Therefore, the front average inlet angle of the water β_{fa} can be calculated as below:

$$\beta_{fa} = \tan^{-1}\left(\frac{V_m}{u + \frac{g\eta_h H}{2u}}\right) \tag{2-20}$$

The calculating method of the rear average inlet angle of the water β_{ra} is similar with the method of front rotor. Based on the direction of the velocity, the rear average inlet angle of the water β_{ra} can be calculated as below:

$$\beta_{ra} = \tan^{-1}\left(\frac{V_m}{u - \frac{V_{ru1}}{2}}\right) \tag{2-21}$$

With the same method, we can also obtain the calculating equation of the rear average inlet angle of the water β_{ra} , it is shown as below:

$$\beta_{ra} = \tan^{-1}\left(\frac{V_m}{u - \frac{g\eta_h H}{2u}}\right) \tag{2-22}$$

The sixth step is calculating the average velocity. From the fifth step, we can obtain the front average inlet angle of the water β_{fa} and the rear average inlet angle of the water β_{ra}. By these two angles, we can calculate the average velocity of the front rotor and rear rotor.

The front average velocity can be calculated as the following equation:

$$W_{fa} = \frac{V_m}{\sin\beta_{fa}} \tag{2-23}$$

The rear average velocity can be calculated as the following equation:

$$W_{ra} = \frac{V_m}{\sin\beta_{ra}} \tag{2-24}$$

The seventh step is calculating the attack angle.

The attack angle is a key parameter to the small hydro-turbine because the performance will change with the changing of attack angle. The position of the attack angle is shown in Figure 2-7.

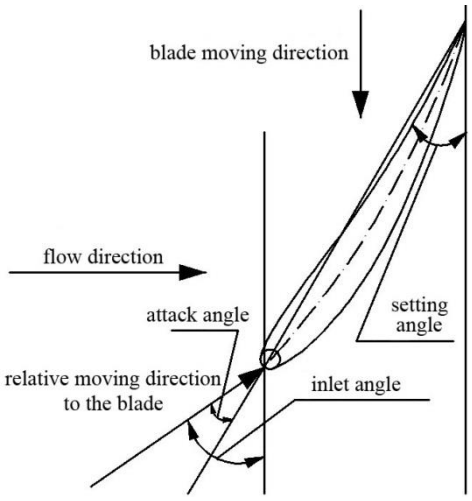

Figure 2-7 The position of the attack angle

From Figure 2-7, we can see that the attack angle can be calculated by inlet angle and setting angle. The setting angle is confirmed when we finish designing, and the inlet angle can be calculated by the axial velocity and circumferential velocity. Therefore, firstly we can use the axial velocity and circumferential velocity to calculate the inlet angle. Then we can use the inlet

angle and setting angle to calculate the attack angle. The inlet angle can be calculated as the following:

$$\beta_{in} = \tan^{-1}\left(\frac{V_z}{|u - |V_t|}\right) \tag{2-25}$$

In equation (2-25), β_{in} denotes the inlet angle, V_z denotes the axial velocity, V_t denotes the circumferential velocity, u denotes the velocity of the blade. u can be calculated as following:

$$u = r * 2\pi * \frac{2300}{60} \tag{2-26}$$

In equation (2-26), u denotes the velocity of the blade. r denotes the section located radius. After obtaining the inlet angle, we can calculate the attack angle. The attack angle can be calculated as the following:

$$\alpha = \beta_{in} - \theta \tag{2-27}$$

In equation (2-27), α denotes the attack angle, β_{in} denotes the inlet angle, θ denotes the setting angle.

The eighth step is referring to the lift force coefficient.

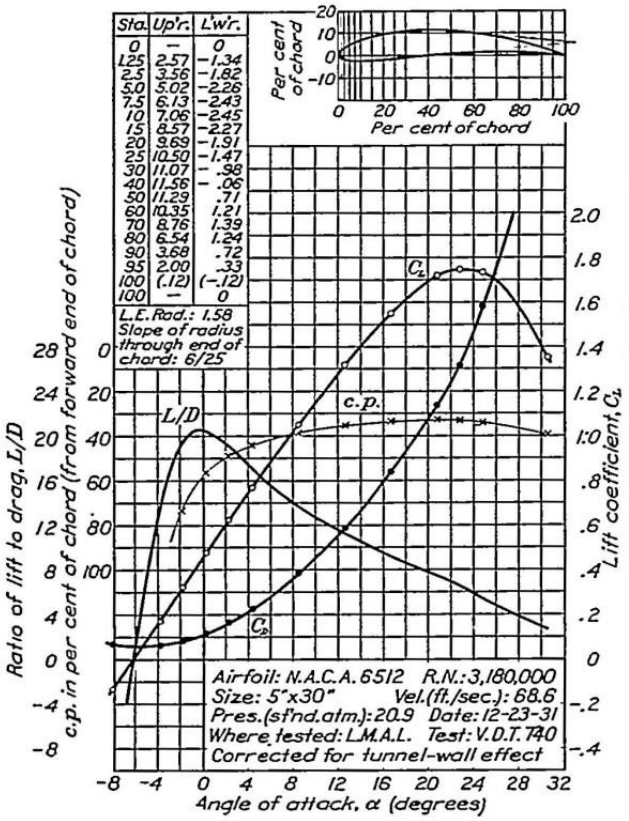

Figure 2-8 The coefficient curves of NACA6512

The coefficient curves of NACA6512 are shown in Figure 2-8.

The lift force coefficient can be obtained by the coefficient curves of NACA6512 because the wind tunnel experiment of this type of blade has been conducted by the NACA. We can use these experiment results into our design.

The ninth step is calculating the multiplying between the lift force and chord. We can obtain the lift force coefficient from the eighth step. Therefore, we can calculate the multiplying between the lift force and chord. We can use the Joukowski's theorem to calculate the lift force of the blade, and the equation is shown as below:

$$C_L = \frac{L}{\frac{1}{2}\rho|V_\infty|^2 l} \tag{2-28}$$

We can use the equation into our contra-rotating small hydro-turbine, and a small part of the blade can also use this equation, the calculating can be shown as below:

$$C_L \times l = \frac{2Z}{\rho \times W_\infty{}^2} \times \frac{dL}{dr} \tag{2-29}$$

The tenth step is deciding the length of the chord. We can obtain the chord because we have obtained the multiplying between the lift force and chord.

After the above 10 steps design, we can decide the basic parameters of this contra-rotating small hydro-turbine. The design efficiency of this contra-rotating small hydro-turbine is 65%, and we will optimize the design and try to enhance the performance and internal flow condition of this contra-rotating small hydro-turbine.

The basic parameters of the rotors are shown in Table 2-2:

Table 2-2 The basic parameters of the rotor

		Hub	Mid	Tip
Front Rotor	Diameter[mm]	29	43.5	58
	Blade Number	4		
	Blade Profile	NACA6512		
	Solidity	1.4	1.07	0.85
	Stagger Angle[°]	25.5	20	15.8
Rear Rotor	Blade Number	3		
	Blade Profile	NACA6512		
	Solidity	0.86	0.71	0.59
	Stagger Angle[°]	44.6	29.1	18.9

The diameter of the rotor is 58mm, and that of casing is 60mm, thus the tip clearance is 1mm. A mouse is beside the rotors to be compared. The hub tip ratio of the front and rear rotor is $D_{hf}/D_{tf}=D_{hr}/D_{tr}=0.5$. All of the design parameters are based on the power, head, flow rate and rotation speed. In this research, the blade number of front and rear rotor should be co-prime in order to suppress the interaction of the blade rows. Then for the front rotor $Z_f=4$ and for the rear rotor $Z_r=3$. The blade type NACA65 serious is chosen to be the profile of the blade. A guide vane is not set at the inlet of the front rotor because the test turbine is designed as compact as possible.

2.2.3 The stacking of the blade

The NACA6512 is just 2D blade profile. The blade has to be stacked to form the 3D blade. There are six 2D airfoil profiles in 6 different positions to be stacked to form the 3D blade. The six 2D airfoil profiles in six different positions are shown in Figure 2-9, and the forming process of the stacking is shown in Figure 2-10:

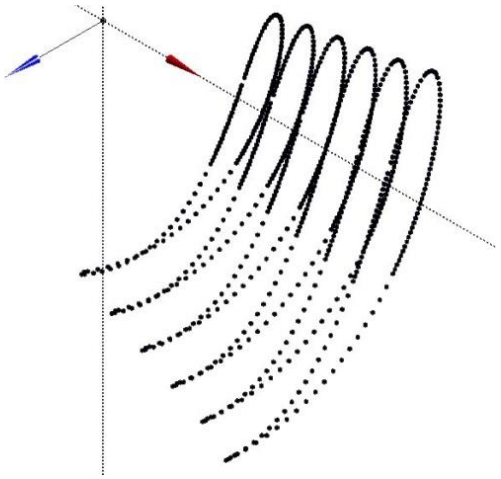

Figure 2-9 Airfoil profile in 6 different positions

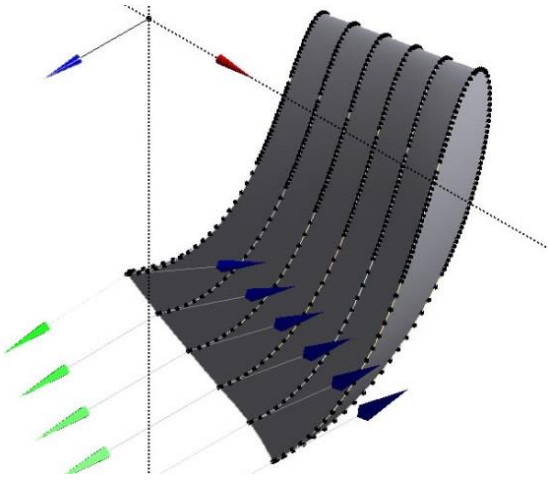

Figure 2-10 The forming process of the stacking

There are four blades onto the front rotor and three blades on the rear rotor, the blade number are co-prime to prevent the interference between the front and rear blade.

2.2.4 The new blade and front rotor

In order to improve the performance of this contra-rotating small hydro-turbine, a new test turbine is designed and manufactured. Compared with the original test turbine, the blade thickness and the shape of front hub of the new test turbine are changed to improve the performance and internal flow condition. On one hand, the blockage ratio of the new blade at radial direction is kept to be constant, so that the blade thickness changes during the whole radial direction. On the other hand, the length of front hub is designed to be longer than that of the original model, and the chamfer of the front hub is changed from flat plane to curved surface, so that flow direction will be changed more slowly and smoothly. The performance experiment and numerical analysis are conducted based on the new test turbine, and the differences between the original model and new model are shown and investigated.

Compared with original test turbine, the new test turbine has two differences with the original model. Firstly, the shape of the front hub is different. The chamfer of the original front rotor is a flat plane, while the chamfer of the new front rotor is a curved surface, and the length of the new front hub is longer than the original front hub. Secondly, the blade thickness of the original front and rear rotor always keep to 12% of the blade length. Here we define a parameter of the blade, which is named as blockage ratio. The blockage ratio is defined as the following,

$$B = \frac{2\pi r - z\dfrac{t}{\sin\theta}}{2\pi r} \times 100\% \qquad (2\text{-}30)$$

In equation (2-30), B denotes the blockage ratio, r denotes the radius of the rotor, z denotes the blade number of the rotor, t denotes the blade thickness, θ denotes the setting angle of the blade. As the equation shown, when the blockage ratio becomes larger, the blade thickness will become smaller. For the flow passage, when the blade thickness becomes smaller, the flow passage between the near two blades will become wider. Therefore, the blockage ratio of the original model changes in the radial direction because r is changed, and the blockage ratio will become larger with the increasing of the radius.

Table 2-3 The original blockage ratio and blade thickness of the front rotor

R [mm]	Blade thickness [mm]	Blade thickness over blade length [%]	Blockage ratio [%]
29	4.32	12	90.52

26.1	4.08	12	90.05
23.2	3.84	12	89.46
20.3	3.6	12	88.71
17.4	3.36	12	87.71
14.5	3.12	12	86.30

The design method of the new blade is different with the original blade. The new design method is that keep the blockage ratio of the blade constant at the radial direction. Therefore, the blade thickness will not keep 12% of the blade thickness during the radial direction. We want to decrease the blade thickness, and make the flow passage between the near two blades become wider. However, the intensity of the blade has to be considered at the same time, because the large blade thickness can increase the intensity of the blade. Therefore, we have to find a balance point, and this new design method is an attempt to find this balance point.

Table 2-4 The original blockage ratio and blade thickness of the rear rotor

R [mm]	Blade thickness [mm]	Blade thickness over blade length [%]	Blockage ratio [%]
29	4.32	12	92.89
26.1	4.08	12	92.54
23.2	3.84	12	92.10
20.3	3.6	12	91.53
17.4	3.36	12	90.78
14.5	3.12	12	89.73

Table 2-5 The new blockage ratio and blade thickness of the front and rear rotor

R [mm]	Blade thickness over blade length [%]	Blockage ratio of front blade [%]	Blockage ratio of rear blade [%]
29	12.00	90.52	92.89
26.1	11.44	90.52	92.89
23.2	10.80	90.52	92.89
20.3	10.08	90.52	92.89
17.4	9.26	90.52	92.89
14.5	8.31	90.52	92.89

The original blockage ratio and blade thickness of the front rotor is shown in Table 2-3, and

the original blockage ratio and blade thickness of the rear rotor is shown in Table 2-4. Because the blade number is different, so the blockage ratio of front and rear rotor is also different. In order to enlarge the flow passage, we choose the highest blockage ratio of front and rear rotor. According to the new design method, the blockage ratio during the radial direction is the same, and the percentage of blade thickness over blade length is changing. The new blockage ratio and blade thickness of front and rear rotor are shown in Table 2-5.

2.3 The design of spacer and spoke

The setting angle of the rear rotor was calculated by the design efficiency of the front rotor (η_{id}=65%), and it was determined on the assumption that the swirling flow downstream of the front rotor directly passed through the flow passage between the front and rear rotor, although there were supporting spokes between the front and rear rotor.

It is planed that the generators are put inside of each front and rear rotor's hub in a product of this kind of small hydro-turbine, and the rotors and generators are supported only by the spokes. Therefore, the spokes are essential for the actual product. The diameter of the spacer is 29mm, which is the same with the diameter of rotor hub, and the axial length of spacer is 33mm. Four spokes are connected to the spacer and they are equally spaced in circumferential direction.

The previous spoke is cone spoke, and the new spoke is cylinder spoke. The previous cone spoke is shown in Figure 2-11, and the new cylinder spoke is shown in Figure 2-12:

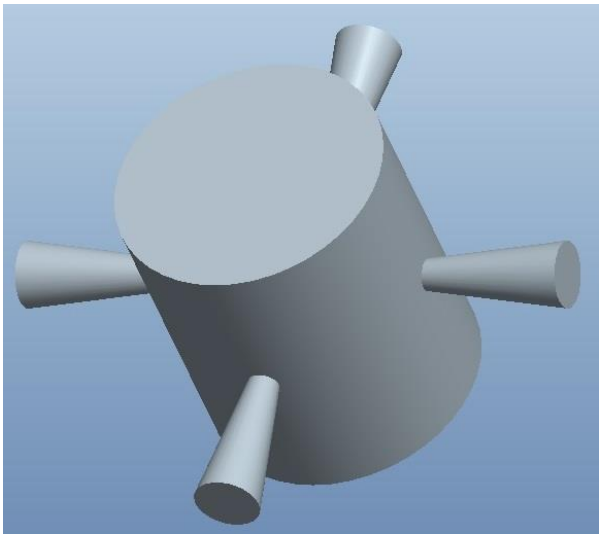

Figure 2-11 The previous cone spoke

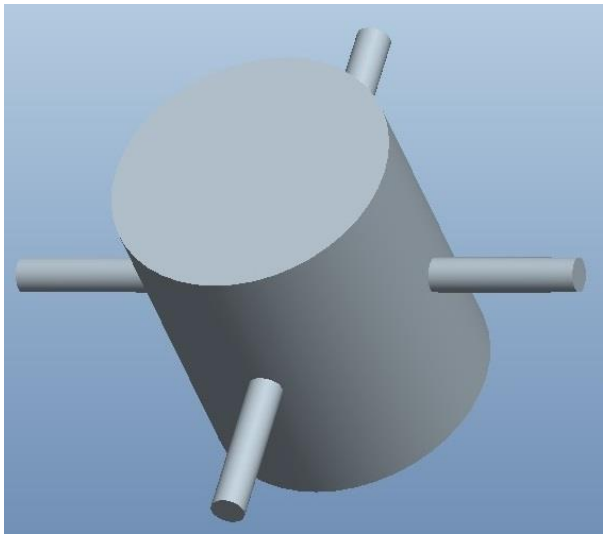

Figure 2-12 The new cylinder spoke

The previous cone spoke was designed to enhance the performance and improve the internal flow condition in a wide flow rate range, and the cone shape is used to keep the blockage ratio in radial direction constant. In previous experiments, it did suppress the wake which generated from the spoke, and made the rear rotor more efficient. However, this kind of cone shape still has disadvantages. For instance, on the viewpoint of materials mechanics, the hub and spoke can be treated as cantilever beam. Based on the mechanics principle, the stress concentration takes place at the hub area, near the spacer. If some fatigue cracks generated, it must be firstly appeared on the hub area of this cone spoke. Thus the larger diameter part of cone spoke is useless for the intensity. Also, large diameter part of cone spoke will result in the large wake zone which will disturb the flow direction in front of the rear rotor. Based on these considerations, we modify the geometry of the spoke from cone to cylinder. The cylinder spoke is expected to achieve higher efficiency in order to increase the performance, and also in order to generate smaller wake zone to improve the internal flow condition.

CHAPTER 3

EXPERIMENT APPARATUS AND MEASUREMENT METHOD

We need to make experiment to clarify the performance of the contra-rotating small hydroturbine. Therefore, we should construct the experiment apparatus of the contra-rotating small hydroturbine. The experiment apparatus can help us to measure the performance of the contra-rotating small hydroturbine. After that, we can use the experiment apparatus to prove the correction of the CFD simulation. If there is no proving, the numerical result will not be believable. In this chapter, we will introduce the details of the experiment apparatus, and introduce the components of this experiment apparatus.

3.1 The introduction of the experiment apparatus

The experiment apparatus is to simulate the working environment of the contra-rotating small hydroturbine. The experiment apparatus are shown in Figure 3-1:

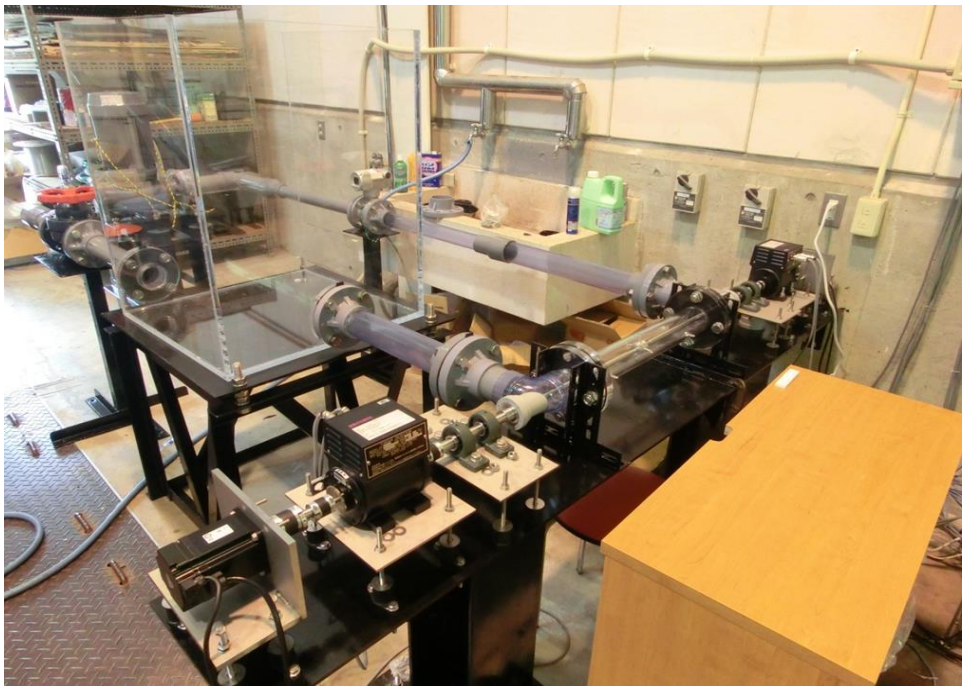

Figure 3-1 The experiment apparatus of the contra-rotating small hydroturbine

The experiment apparatus is a circulatory system, and it consists of many casings. The fluid media is water, and the water flow into the casing, it simulates the working experiment of the contra-rotating small hydroturbine. Because the working environment of the contra-rotating small

hydroturbine is the water supplying system in the farm land, the test turbine is assembled into the casing. This will simulate the working environment of the contra-rotating small hydroyurbine, and obtain the accurate performance experiment data of the test turbine. The schematic diagram of the experiment apparatus is shown in Figure 3-2:

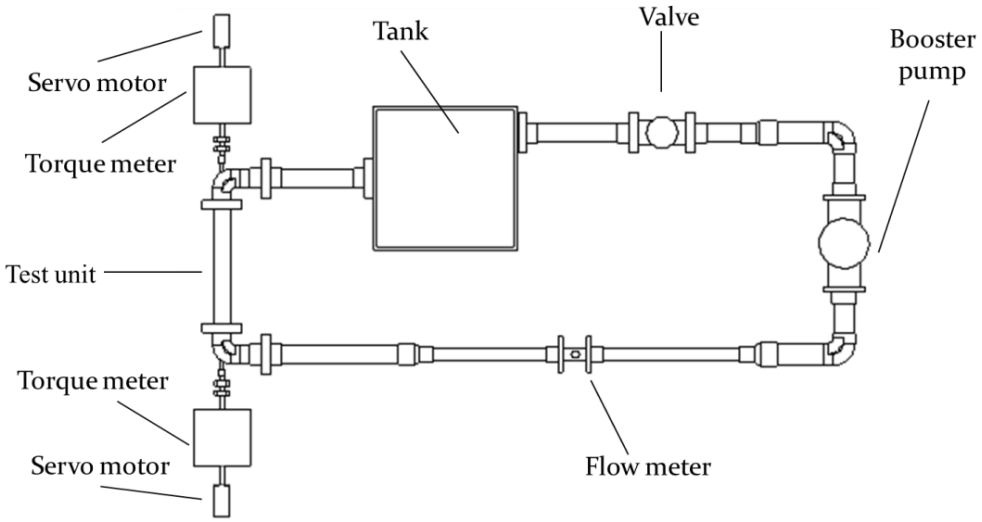

Figure 3-2 The schematic diagram of the experiment apparatus

The detailed size of the experiment apparatus is shown in Figure 3-3:

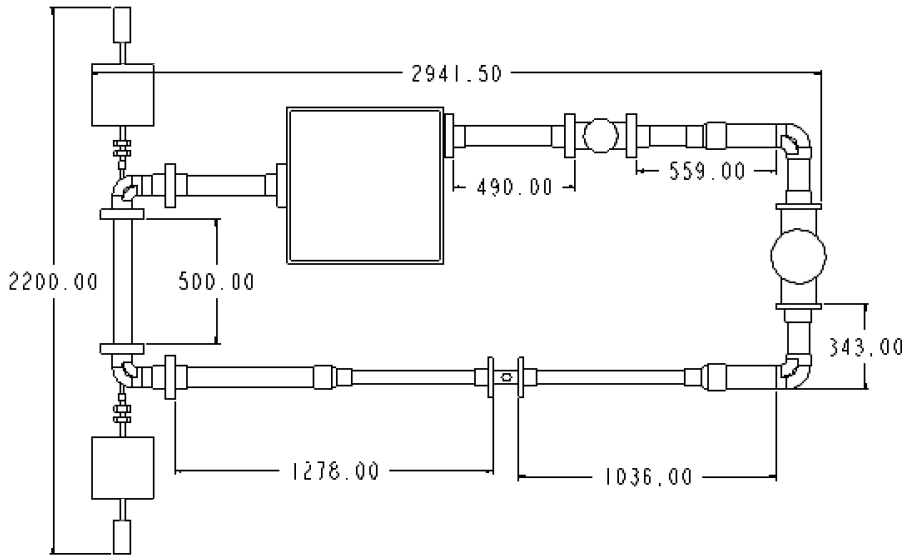

Figure 3-3 The detailed size of the experiment apparatus

The test section was made of a transparent acrylic resin for visualization experiments. The

fluid media is water, and the static head differences on the casing wall between about 2*D* upstream of the front rotor and about 2*D* downstream of the rear rotor are measured for head evaluation. Each rotor is connected to a respective shaft and driven by a respective motor set upstream and downstream of the test section. The length of the transparent test section is 500mm and straight pipes over 4*D* are ensured upstream and downstream of the test rotors to suppress the influence of the swirl flow from the 90 °bend near the test section.

The test turbine is assembled into the casing, just like it is into the casing of water supplying system in farm land. The assembled test turbine is shown in Figure 3-4:

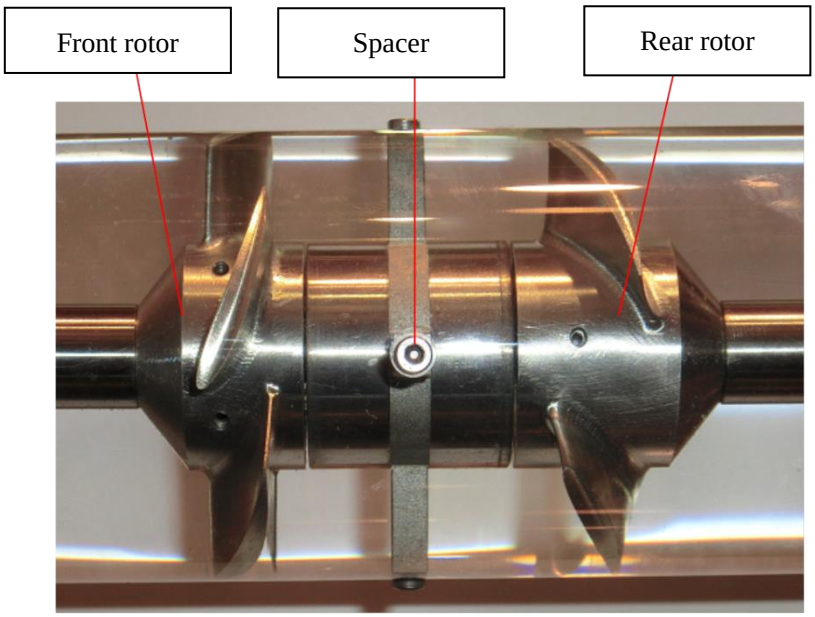

Figure 3-4 The assembled test turbine

As a constant value, rotation speed of the front and rear rotor is N_f=N_r=2300r/min. The flow rate *Q* is obtained by a magnetic flow meter KEYENCE FD-UH50H installed far downstream of the hydro-turbine and the measurement accuracy of it is ±0.5%. Then torque of each front and rear rotor is measured by a respective torque meter ONO SOKKI SS050 and its measurement accuracy is ±0.5%. Then, a shaft power is calculated by the torque and rotation speed which is measured by a rotation speed sensor ONO SOKKI MP-981. The shaft power is evaluated by the torque eliminating the mechanical loss in this performance experiment. Hydraulic efficiency of the hydro-turbine is calculated as the ratio of the shaft power to the water power.

3.2 The other components

3.2.1 The servo motor

There are two servo motors in each side of the casing where the test turbine is assembled in,

and the servo motors drive the front rotor and rear rotor. The servo motors are controlled by PLC controlling unit, and there are two shafts that are connect with the front rotor and rear rotor. One of the servo motor is shown in Figure 3-5:

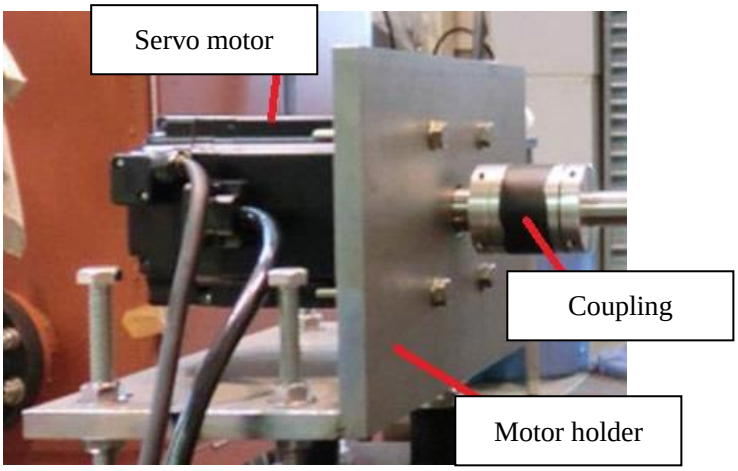

Figure 3-5 One of the servo motor

The basic parameters of the servo motor are shown as below:

Table 3-1 The basic parameters of the servo motor

Company	Keyence
Type	SV-M075CS
Power	750
Torque	2.39
Maximum Torque	8.36
Current	4.7
Maximum current	16.9
Rotation speed	3000
Maximum rotation speed	6000
Torque per step	0.544
Moment of inertia	1.57
Power per second	36.3
Angle per second	15200
Exciting mode	Permanent magnet
Insulation resistance	Above DC500V 10MΩ

3.2.2 The casing

The test turbine is assembled into the casing. The test section casing is made of a transparent acrylic resin for visualization experiments. Therefore, we can see the experiment process and running process of the test turbine. We can also observe the running status of the test turbine through the transparent test section casing. The transparent test section casing is shown in Figure 3-6:

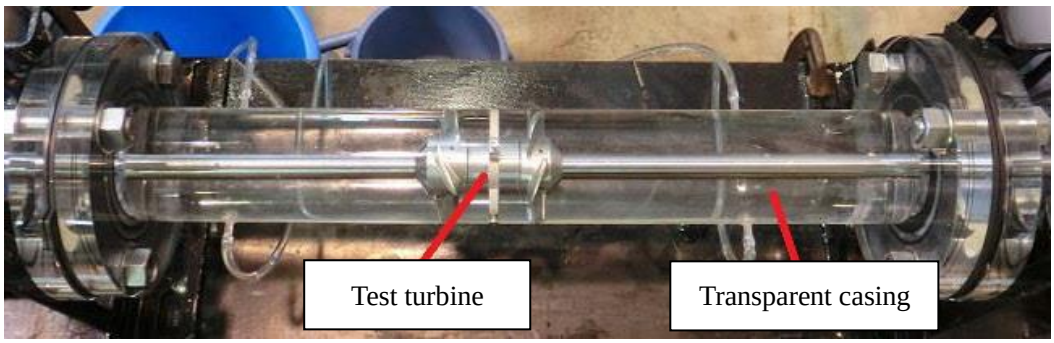

Figure 3-6 The transparent casing

The experiment apparatus also includes other casings. Some of the casing is transparent, and some of the casing is not transparent. Sometimes we should observe the flow conditions into the casing. The casings are shown in Figure 3-7:

(a)Casing 1

(b)Casing 2

(c)Casing 3

(d)Casing 4

(d)Casing 5

Figure 3-7 All of the casings into the experiment apparatus

3.2.3 The boost pump

The water flows into the casing, and the boost pump is the driving components of system. The boost pump is driven by the three-phase asynchronous motor, and they are far from the transparent casing. Besides, we need to change the flow rate during the experiments. Therefore, we need to change the rotating speed of the three-phase asynchronous motor, then the rotating speed of the boost pump is changed, and finally the flow rate of the water is changed. In order to change the rotating speed of the three-phase asynchronous motor, we use a frequency changer in

this experimental apparatus.

The boost pump and motor are shown in Figure 3-8, and the frequency changer is shown in Figure 3-9:

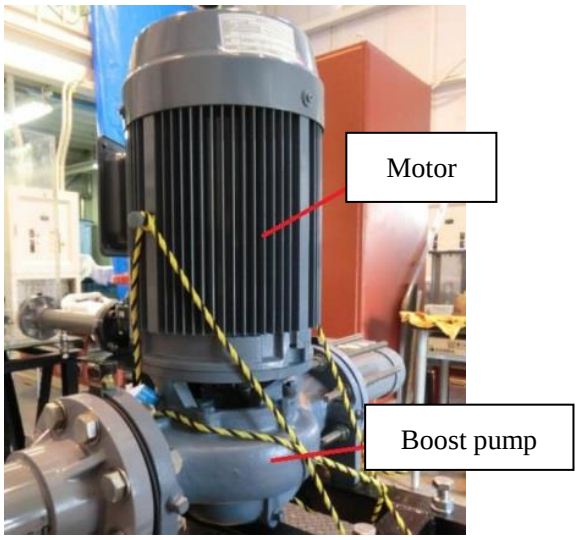

Figure 3-8 The boost pump and motor

Figure 3-9 The frequency changer

The basic parameters of the boost pump are shown in Table 3-2:

Table 3-2 The basic parameters of the boost pump

Company	EBARA
Type	80LPD65.5A
Power supply	Three-phase asynchronous motor
Power [kW]	5.5
Displacement [L/min]	500
Head of delivery [m]	27.5
Displacement [L/min]	1400
Head of delivery [m]	15
Noise [dB]	65
Authorized pressure [MPa]	0.67

3.2.4 The tank

The experiment needs some water to flow into the casings. Therefore, the experiment apparatus need a tank to hold the water. Besides, during the experiments we also need some

water to reduce the fluctuation of the water. However, it is difficult to fulfill the requirement of the experiments only by the water in the casings. Therefore, a water tank, which is aiming at supplying the water and reducing the fluctuation of the water, will be necessary for the experiments.

The tank is also made of a transparent acrylic resin for visualization experiments, and this is convenient for us to observe the running status of the test turbine. The water tank is adopted for the structure of cube, and it doesn't have a lid. The water is directly contacted with the atmosphere.

Before the experiment, we will fill enough water into the tank. The water tank is shown in Figure 3-10:

Figure 3-10 The transparent tank

3.3 The measurement method

3.3.1 The flow meter

The flow meter is for measuring the flow rate of the water. The flow meter is the key components. We need to change the flow rate when we make performance experiment, and we need to use the flow meter to measure the flow rate.

During the experiments, firstly we need to change the frequency of the frequency changer in order to control the rotating speed of the three-phase asynchronous motor. If the rotating speed of

the three-phase asynchronous motor is controlled, the rotating speed of the boost pump is also controlled. Secondly, we need to check the measuring value of the flow meter, and modify the frequency of the frequency changer. Then the rotating speed of the boost pump is controlled, and finally the flow rate of the water is controlled. We will keep modifying the frequency of the frequency changer until we obtain the suitable flow rate of the water. Therefore, we need the flow meter to measure the flow rate of the water in order to judge that whether the flow rate is the suitable flow rate.

The flow meter is shown in Figure 3-11:

Figure 3-11 The flow meter

The basic parameters of the flow meter are shown in Table 3-3:

Table 3-3 The basic parameters of the flow meter

Company	KEYENCE
Type	FD-UH50H
Flange type	JIS 10K
Type of diameter	50A
Range of measurement	3%-100% of the setting measurement
Setting maximum flow rate [L/min]	1178.1
Setting initial flow rate [L/min]	500
Accuracy	±0.5%
Temperature of measuring fluid	-10-+100℃

Range of measuring pressure [MPa]	1
Unit of flow rate	L/min

The installing position of the flow meter is downstream the boost pump, and the installing position of the flow meter is far from the test turbine. Because the wake will be generated downstream the test turbine, the installing position of the flow meter should be far from the test turbine to avoid the influence of the wake. The flow meter needs a stable flowing condition to measure the flow rate of the water. Besides, the flow meter should be checked when its measuring value is stable.

3.3.2 The torque meter

There are two torque meters in the experimental apparatus, and these two torque meters are connected with the two driving shafts respectively.

The torque meter can measure the torque generated from the contra-rotating small hydroturbine, and then we can use the data of torque meter to calculate the power and efficiency of the contra-rotating small hydroturbine. The front torque meter is connected with the front rotor, and the rear torque meter is connected with the rear rotor. The bearing is connected with the torque meter by the coupling.

The torque meter is shown in Figure 3-12:

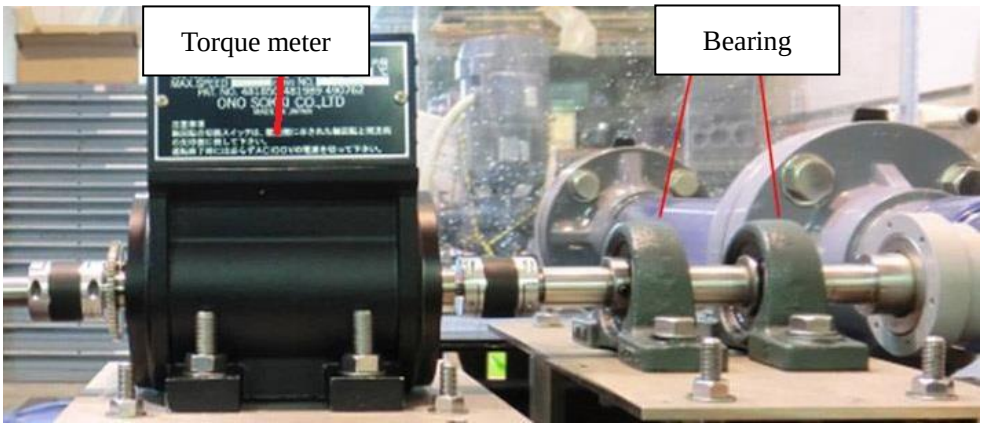

Figure 3-12 The torque meter

The basic parameters are shown in Table 3-4，these two torque meters are the same type for the servo motors are also the same.

Table 3-4 The basic parameters of the torque meter

Company	ONO SOKKI

Type	SS050
Range [N×m]	5
Min Measuring Unit [N×m]	1
Range of rotating speed	0-6000
Moment of inertia [kg/m^2]	4.25×10^{-5}
Accuracy	±0.5%
Suitable rotating speed sensor	MP-981
Power supplying	Ac100V
Range of measuring temperature	0-40℃

3.3.3 The rotation speed sensor

The rotation speed sensor can help us to know the rotation speed of the contra-rotating small hydroturbine. It is installed with the torque meter. A plate with many saw teeth is also installed with the torque meter. This is plate is to help the rotation speed sensor to measure the rotation speed of the contra-rotating small hydro-turbine. The rotation speed sensor and the torque meter are auxiliary product and they are from the same company. The company supports the matched sensors for experimental apparatus.

The rotation speed sensor is shown in Figure 3-13:

Figure 3-13 The rotation speed sensor

The rotation speed sensor can output the electrical signal to the plate, and the saw teeth on the plate are to reflect the electrical signal which is output from the rotation speed sensor. Then the rotation speed sensor receives the signal which is reflected by the plate. By means of calculating the changing frequency of the electrical signal, the rotating speed of the shaft can be calculated by the sensor. Because the driving shaft is connected with the rotor of the contra-rotating small hydroturbine, we can know the rotating speed of the test turbine. This is the

principle of the rotation speed sensor.

The basic parameters of the rotation speed sensor are shown in Table 3-5:

Table 3-5 The basic parameters of the rotation speed sensor

Company	ONO SOKKI
Type	MP-981
Module	0.5-3
Range [Hz]	1-20
Output impedance	330Ω
Protection circuit	Power polarity protection
Maximum voltage	DC250V
Mass [g]	80

3.3.4 The pressure sensor

There are two pressure sensors in the experiment apparatus, and they are assembled on the transparent casing. One of the pressure sensor is assembled on the upstream of the test turbine, and the other pressure sensor is assembled on the downstream of the test turbine. The pressure sensors are connected with the small hole of the test section casing.

The position of the small hole on the test section casing is shown in Figure 3-14:

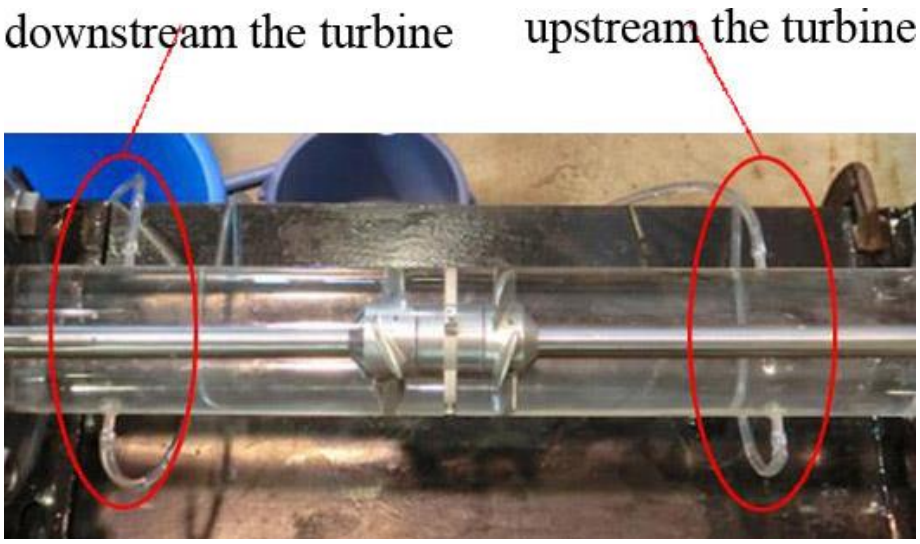

Figure 3-14 The position of the small hole on the test section casing

The pressure sensors are to help to measure the pressure difference between two positions of

the hole. Then the head of the test turbine can be calculated by the pressure difference. A tube is used to connect the hole and the pressure sensor. There are totally 4 holes on the test section casing. Two of the holes are connected with the tube, and one pressure sensor is connected with the tube.

The pressure sensor is shown in Figure 3-15:

Figure 3-15 The pressure sensor

The basic parameters of the front pressure sensor are shown in Table 3-6, and the basic parameters of the rear pressure sensor are shown in Table 3-7:

Table 3-6 The basic parameters of the front pressure sensor

Company	Kyowa
Type	PGMC-A-500KP
Range [KPa]	500
Natural vibration [KPa]	34
Range of temperature compensation	0-50℃
Maximum measuring value	150%

Table 3-7 The basic parameters of the rear pressure sensor

Company	Kyowa
Type	PGMC-A-200KP
Range [KPa]	200
Natural vibration [KPa]	34

Range of temperature compensation	0-50℃
Maximum measuring value	150%

3.4 The data acquisition system

The data acquisition system receives the data which are measured from the different sensors, and they can also save the data and export the data when we need to know them. The data acquisition system includes the data acquisition module and the torque meter module which is matched for the torque meter.

The key component of the data acquisition system is the data acquisition module, and the data acquisition module is shown in Figure 3-16:

Figure 3-16 The data acquisition module

There are four channels in the data acquisition module. Two channels are for pressure sensors. The other two channels are for torque meters. The data acquisition frequency of the data acquisition module is enough for the experiments, and the storage space is also enough for the experiments data. When we make experiments, we will output all of the data in the data acquisition module.

The basic parameters of the data acquisition module are shown in Table 3-8:

Table 3-8 The basic parameters of the data acquisition module

Company	Kyowa
Type	EDS-400A
Range of temperature	0-50℃

Supplying power	DC10-16V
Range of saving temperature	-10-60℃
Mass [g]	500g
Number of channels	4
Accuracy	±0.5%
Input voltage	±10V
Maximum input voltage	±30V
Resolution of the AD converter	16bit
Bridge voltage	DC2V

The torque meter module is matched instrument for the torque meter. It can display the rotation speed of the rotor and the torque of the shaft, and it can receive the data transformed by the torque meter and the rotation speed sensor.

The torque meter module is shown in Figure 3-17:

Figure 3-17 The torque meter module

CHAPTER 4

NUMERICAL METHOD AND CONDITIONS OF SIMULATION

When we finish the design of the contra-rotating small hydroturbine, next we should use the design model to make CFD simulation to predict its performance. In this chapter, we introduce the numerical method and conditions of CFD simulation. The detailed information about the numerical simulation is introduced in this chapter.

4.1 The introduction of numerical simulation

Computational fluid dynamics (short for CFD) is an important research direction of the fluid dynamics. It is a new interdiscipline that is high developed with the developing of computer science. Before the CFD simulation, the fluid dynamics is only consist of theoretical fluid dynamics and experimental fluid dynamics. However, the theoretical fluid dynamics and experimental fluid dynamics have their own disadvantages. The CFD simulation can overcome the disadvantages of the theoretical fluid dynamics and experimental fluid dynamics, therefore, the CFD simulation is getting more and more attention.

The basic equation of the Computational fluid dynamics is the same with the theoretical fluid dynamics, it is Navier-Stokes equation. The equation is shown as below:

$$\begin{cases} \dfrac{\partial(\rho u)}{\partial t} + div(\rho u \boldsymbol{V}) = \dfrac{\partial}{\partial x}\left(\mu \dfrac{\partial u}{\partial x}\right) + \dfrac{\partial}{\partial y}\left(\mu \dfrac{\partial u}{\partial y}\right) + \dfrac{\partial}{\partial z}\left(\mu \dfrac{\partial u}{\partial z}\right) - \dfrac{\partial p}{\partial x} + S_u \\ \dfrac{\partial(\rho v)}{\partial t} + div(\rho v \boldsymbol{V}) = \dfrac{\partial}{\partial x}\left(\mu \dfrac{\partial v}{\partial x}\right) + \dfrac{\partial}{\partial y}\left(\mu \dfrac{\partial v}{\partial y}\right) + \dfrac{\partial}{\partial z}\left(\mu \dfrac{\partial v}{\partial z}\right) - \dfrac{\partial p}{\partial y} + S_v \\ \dfrac{\partial(\rho w)}{\partial t} + div(\rho w \boldsymbol{V}) = \dfrac{\partial}{\partial x}\left(\mu \dfrac{\partial w}{\partial x}\right) + \dfrac{\partial}{\partial y}\left(\mu \dfrac{\partial w}{\partial y}\right) + \dfrac{\partial}{\partial z}\left(\mu \dfrac{\partial w}{\partial z}\right) - \dfrac{\partial p}{\partial z} + S_w \end{cases} \tag{4-1}$$

The equation of the mass flow conservation and Reynolds Averaged Navier-Stokes equation are solved by the finite volume method in ANASYS-CFX.

4.2 The turbulence model

The turbulence model is the basic option of the CFD simulation. There are a lot of turbulence models to choose, and we should choose a suitable turbulence model based on the condition of our CFD simulation. The standard k-Epsilon model is the most useful turbulence model in the engineering CFD simulation. Therefore, we choose the k-Epsilon model in our

contra-rotating small hydroturbine CFD simulation.

The simulation is conducted under the condition of 3D unsteady flow condition. The fluid is assumed to be incompressible and isothermal water. The equation of the mass flow conservation and Reynolds Averaged Navier-Stokes equation are solved by the finite volume method in ANSYS-CFX. The standard wall function is utilized near the wall.

4.3 The near wall condition

We use the standard wall function in the CFD simulation of contra-rotating small hydroturbine. The Scalable Wall Function of the CFD simulation is shown as below:

$$v^* = C_\mu^{1/4} k^{1/2} \tag{4-2}$$

In the equation:

$$v_\tau = \frac{V_\tau}{\frac{1}{k}\ln(y^*) + C} \tag{4-3}$$

We choose the blade area to refine the mesh because the blade is complicated geometry and the physical quantity is changed a lot at blade area. We set up a refinement to all of the blades of the front rotor and rear rotor, and we define the maximum grid size at this refinement area is 0.35mm. Therefore, the grid at blade area is refined. Besides, we set up an inflation layer at the outside surface of the rotor. The thickness of this inflation layer is 1mm. About the value of y+, it is less than 100 and bigger than 50 at most of the domains. The maximum of y+ is 230 at a small part of areas which are difficult to mesh.

4.4 The high resolution scheme and residual

We use the ANSYS CFX as the software of the CFD simulation. In CFX, the below equation can show the high resolution scheme.

$$\phi_{tp} = \phi_{up} + \beta \nabla \phi \cdot \Delta \vec{r} \tag{4-4}$$

The residual is the judgement standard of the CFD simulation. The software will stop the iteration by judging the residual, when the residual of the calculation is lower than the residual standard, CFX will stop the iteration by itself. Therefore, we should set a suitable residual standard, if the standard is too small, the CPU will be wasted by too much calculation. If the standard is too large, the calculation result will not be accurate.

In this simulation, the residual is set up to be 10^{-4}. When the residual is smaller than 10^{-4}, the software will stop the calculation. However, sometimes the residual can't reach to the value

which we have set up in the pre-process. Sometimes, the residual tend to be constant, but the value is larger than the setting up value. Therefore, the software will not stop the calculation. The calculation will continue to the setting number of iteration. When the calculation reaches to the number of iteration and the residual is constant, we still think that the result is convergent, and we can use the result to make analysis.

4.5 The analysis model and meshing

The numerical analysis model is built. The numerical model is designed to be the same with test section and included the inlet and outlet bend of the experimental apparatus. Straight pipes over 4D were ensured for the inlet and outlet pipes, which are designed to be the same with the experimental apparatus, in order to suppress the influence of the bend near the inlet and outlet pipes. Each front and rear rotor is connected and driven by a shaft, these two shafts are modeled in the numerical analysis and rotated in the contrary direction respectively. The constant velocity which is vertical to the inlet boundary and the constant pressure are given as the boundary condition at inlet and outlet respectively.

The coupling among the front rotor, spokes and rear rotor regions is accomplished by the transient rotor/stator. The time step number per rotation of front and rear rotor is 120 and the time step is t=2.174×10^{-4}s. The data of one rotation is obtained after 5 rotations in unsteady numerical analysis.

The numerical grids of the whole domains in ANASYS-CFX are shown in Figure 4-1:

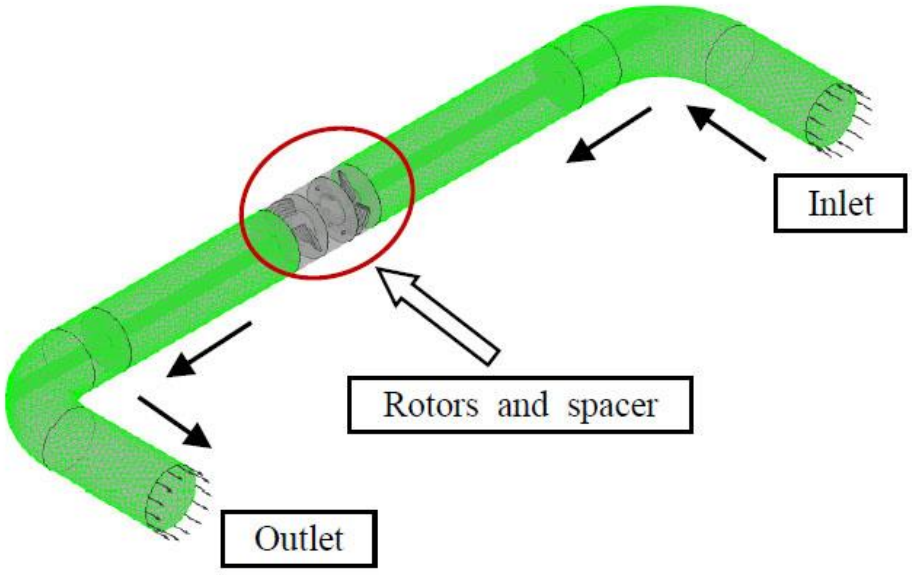

Figure 4-1 The numerical grids of the whole domains

We will show three numerical simulation models, it includes the original model, the new

model and the model of using cylinder spokes.

The grids data of the original model is shown in Figure 4-2:

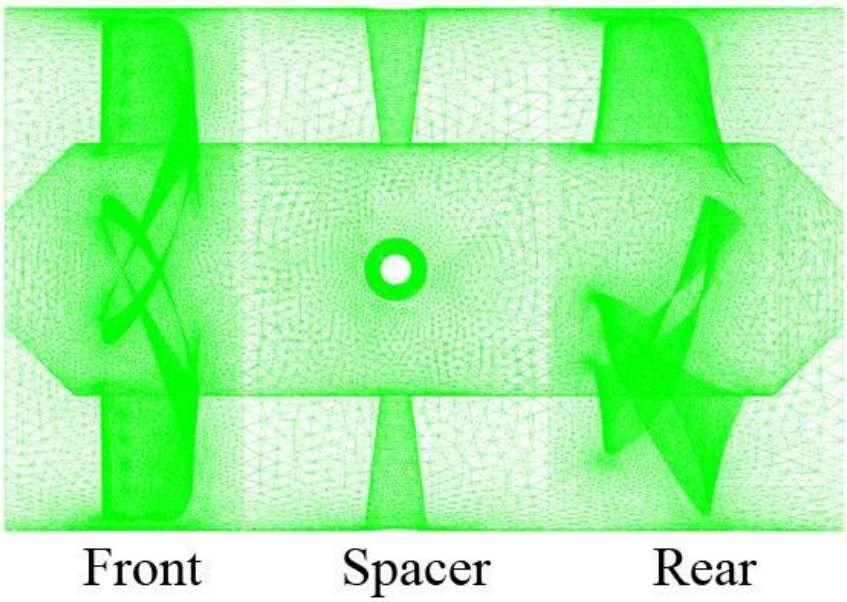

Figure 4-2 The numerical grids of the original model

The grids data of the new model is shown in Figure 4-3:

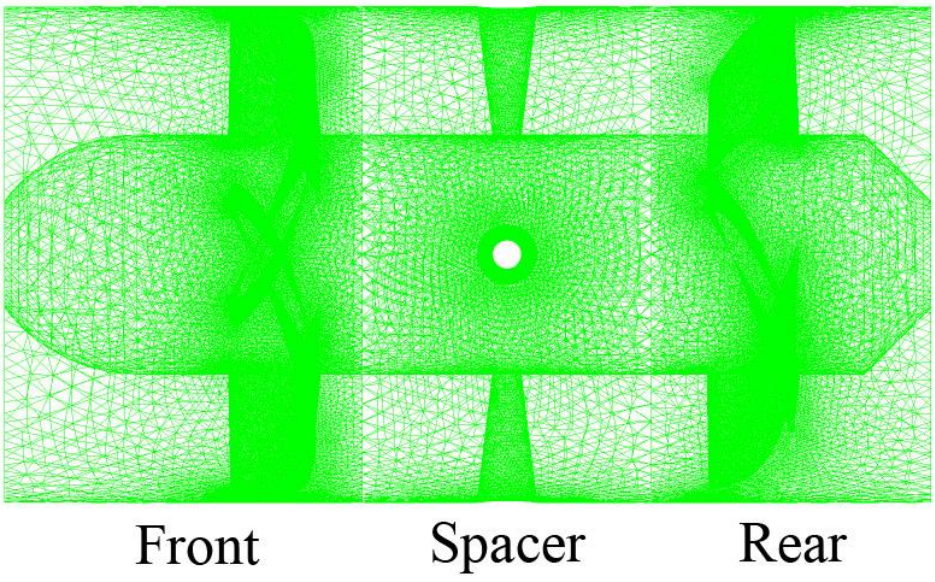

Figure 4-3 The numerical grids of the new model

The grids data of the model using cylinder spokes are shown in Figure 4-4:

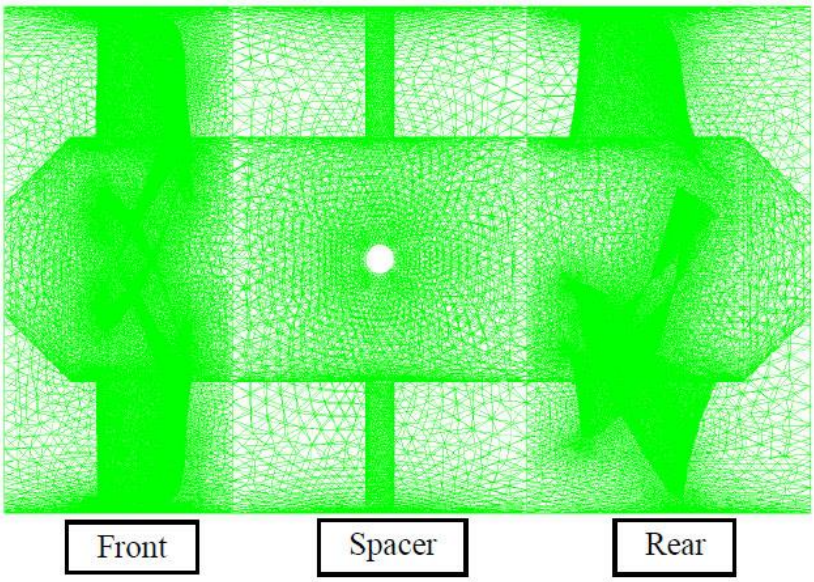

Figure 4-4 The model using cylinder spokes

The whole domains of this numerical analysis consisted of 7 parts, including inlet elbow, inlet casing, front rotor, spacer, rear rotor, outlet casing and outlet elbow. The element number of inlet elbow and inlet casing is 495,241, the element number of rotors and spacer is 6,906,418, the element number of outlet casing and outlet elbow is 316,811. In the case of cone spoke with spacer, the element number of rotors and spacer is 6,861,268, element numbers of other parts are the same with this model. This numerical analysis is performed at 13 flow rate points from 90% to 200% of the design flow rate. These flow rate points are mainly set to large flow rate points because the small hydro-turbine could be operated in large flow rate.

The numerical analysis was conducted by three steps. The first step is steady simulation, after this steady simulation we can get the numerical result of steady state. The second step is unsteady simulation, the front rotor and rear rotor are simulated to rotate in five rotations, then we can get the unsteady result. The third step is the unsteady simulation, this step is to output the simulation data. In the third step the front and rear rotor are simulated to rotate in the last rotation, and the data was output in every time step.

CHAPTER 5

RESULTS AND DISCUSSION

In this chapter, the simulation and experiment of the test turbine with previous cone spoke is conducted, the result of the simulation and experiment is obtained. The numerical simulation and performance experiments of the new model are conducted and they are compared with each other. To compare the performance of the original model and new model, the experimental results of the original model and new model are clarified and compared. The simulation of the test turbine with new cylinder spoke is also conducted, and the result of the simulation is obtained. The comparison between cone spoke and cylinder spoke is clarified. Besides, the foreign vegetable materials experiment is also conducted to clarify the running stability of this contra-rotating small hydroturbine.

5.1 The simulation result of test turbine

5.1.1 The simulation result of original model

To make experiments for the contra-rotating small hydro-turbine, the test turbine of the original model and new model are manufactured.

The original test turbine is shown in Figure 5-1. In the picture, we put a computer mouse beside the test turbine to help others know the real size of the test turbine.

Figure 5-1 The original test turbine

The new test turbine is shown in Figure 5-2. In the picture, we also put a computer mouse beside the test turbine to help others know the real size of the test turbine.

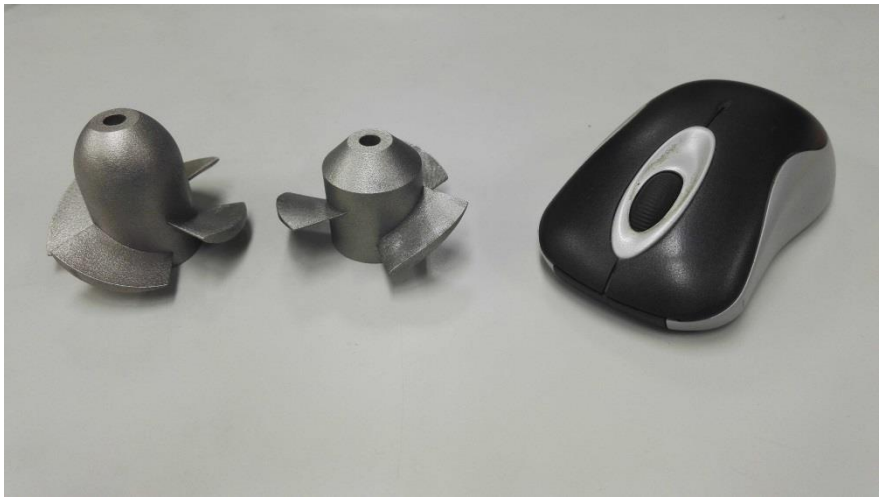

Figure 5-2 The new test turbine

The original test turbine is manufactured by traditional method. The material of the rotor is aluminum, and the rotors are made by cutting. The new test turbine is manufactured by 3D print, and the material is titanium alloy. The simulation result is obtained and it consists of power characteristic, head characteristic, and efficiency characteristic. These three characteristic form the performance of the contra-rotating small hydroturbine.

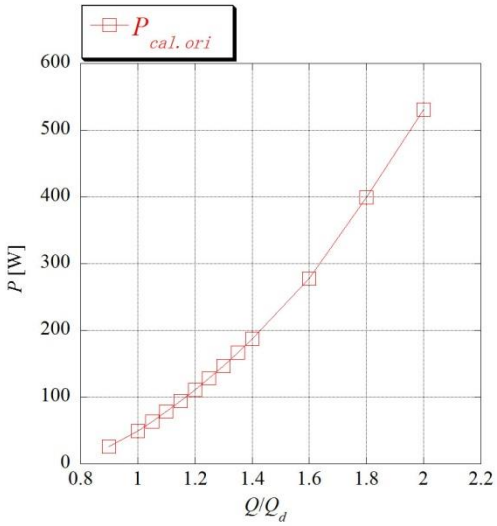

Figure 5-3 The original power characteristic

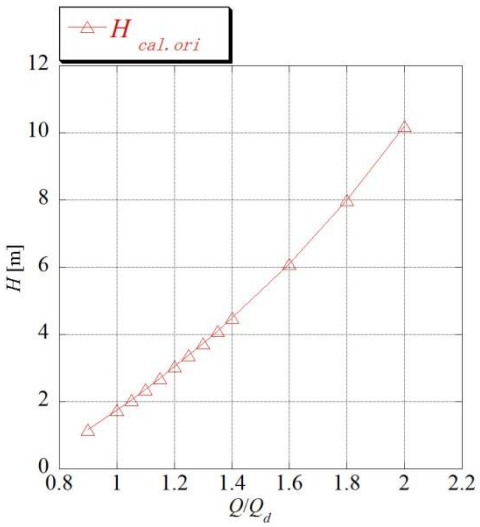

Figure 5-4 The original head characteristic

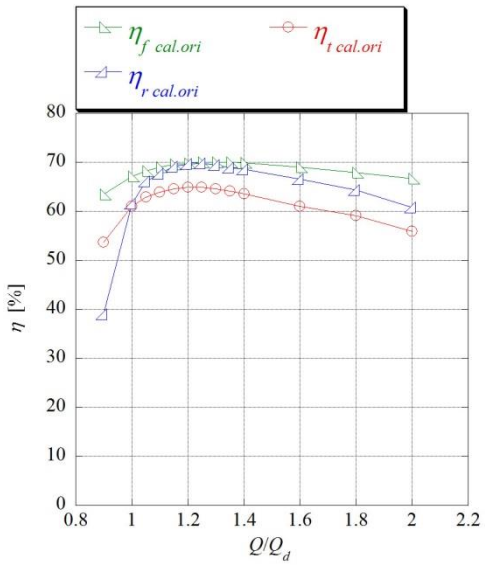

Figure 5-5 The original efficiency characteristic

The power characteristic of the original model is shown in Figure 5-3, the head characteristic of the original model is shown in Figure 5-4, the efficiency characteristic of the original model is shown in Figure 5-5.

In Figure 5-3, Figure 5-4, Figure 5-5, the performance of the original model is clarified. The power increases with the increasing of the flow rate. The head also increases with the increasing of the flow rate. The efficiency firstly increases with the flow rate. Then it reaches to the maximum, after that it decreases with the flow rate.

5.1.2 The simulation result of new model

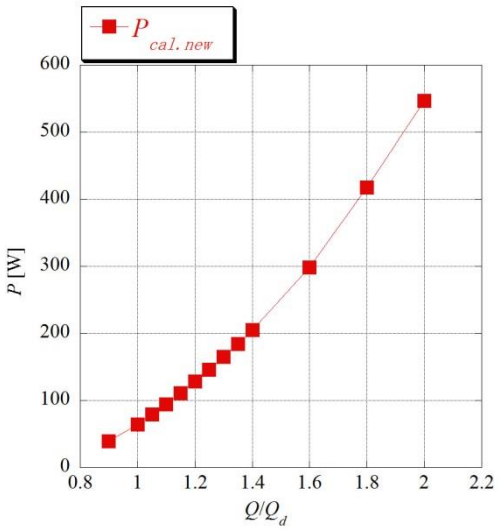

Figure 5-6 The new power characteristic

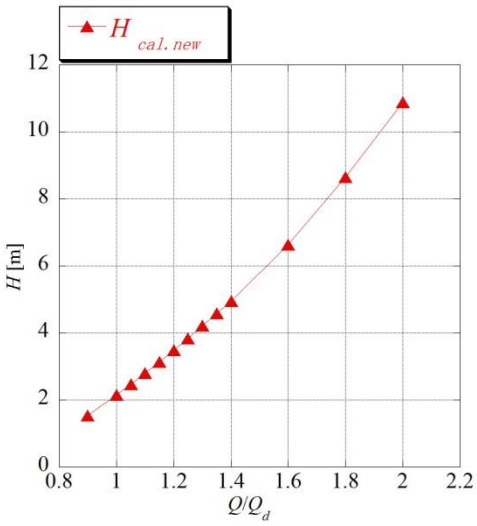

Figure 5-7 The new head characteristic

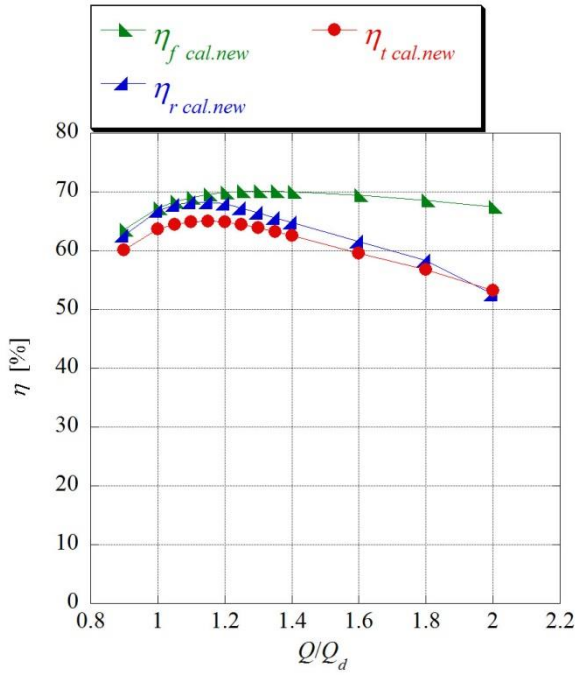

Figure 5-8 The new efficiency characteristic

The power characteristic of the original model is shown in Figure 5-6, the head characteristic of the original model is shown in Figure 5-7, the efficiency characteristic of the original model is shown in Figure 5-8.

In Figure 5-6, Figure 5-7, Figure 5-8, the performance of the new contra-rotating small hydroturbine is clarified. The power increases with the increasing of the flow rate. The head also increases with the increasing of the flow rate. The efficiency firstly increases with the flow rate. Then it reaches to the maximum, after that it decreases with the flow rate. The performance tendency of the new model is the same with the original model.

5.2 The experiment result of test turbine

5.2.1 The experiment result of original model

To prove the correction of the numerical simulation, we make experiments for the original test turbine and original test turbine on the experiment apparatus. The maximum flow rate of the experiment was $1.4Q_d$ because of the limitation of measurement instruments.

The power characteristic of the original model is shown in Figure 5-9, the head characteristic of the original model is shown in Figure 5-10, the efficiency characteristic of the original model is shown in Figure 5-11.

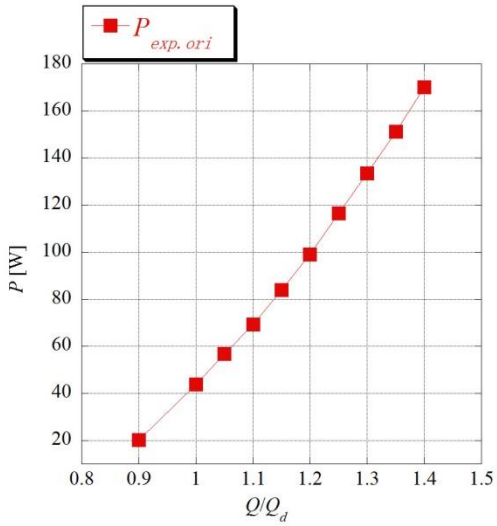

Figure 5-9 The original power characteristic

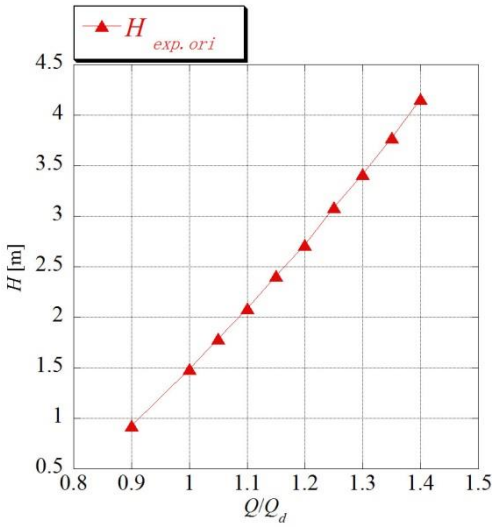

Figure 5-10 The original head characteristic

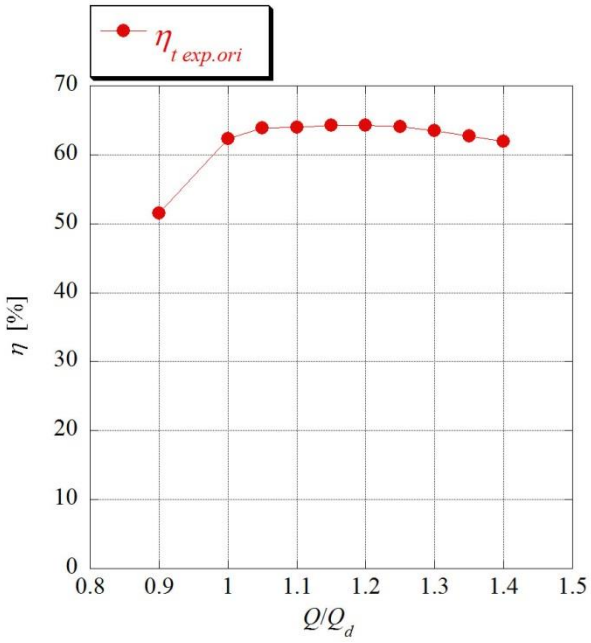

Figure 5-11 The original efficiency characteristic

In Figure 5-9, Figure 5-10, Figure 5-11, the experimental performance of the original model is clarified.

From the experimental result, we can find that the experimental result of the original model is similar to with numerical result of the original model. The power increases with the increasing of the flow rate. The head also increases with the increasing of the flow rate. The efficiency firstly increases with the flow rate. Then it reaches to the maximum, after that it decreases with the flow rate.

The comparison between experimental result of the original model and numerical result of the original model in the previous work is shown in Figure 5-12:

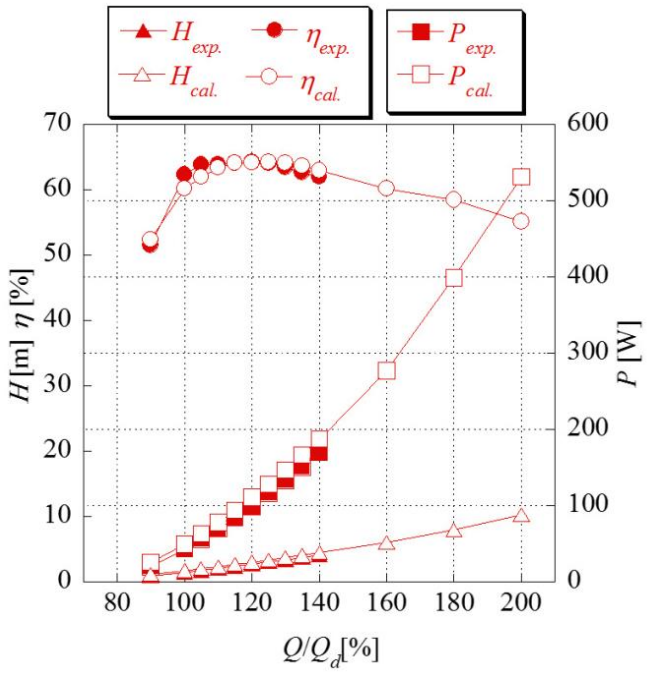

Figure 5-12 The comparison between experimental result and numerical result

The numerical result was compared with the experimental result, and they were well matched with each other. The maximum flow rate of the experiment was $1.4Q_d$ because of the limitation of measurement instruments.

Therefore, the numerical analysis of the original model is proved to be correct, and we can use this numerical model to make some prediction to the original model when we change some parameters of this small hydroturbine.

5.2.2 The experiment result of new model

To prove the correction of the numerical simulation, we also make experiments for the new test turbine and new test turbine on the experiment apparatus. The maximum flow rate of the experiment was $1.4Q_d$ because of the limitation of measurement instruments.

The power characteristic of the new model is shown in Figure 5-13, the head characteristic of the new model is shown in Figure 5-14, the efficiency characteristic of the new model is shown in Figure 5-15.

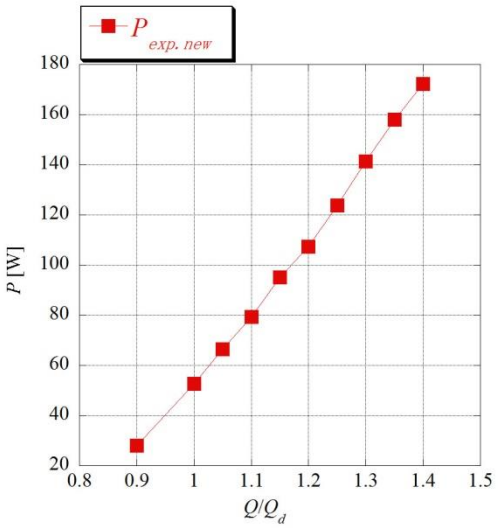

Figure 5-13 The new power characteristic

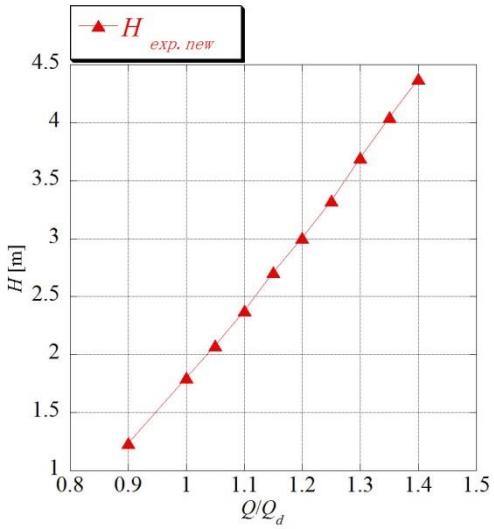

Figure 5-14 The new head characteristic

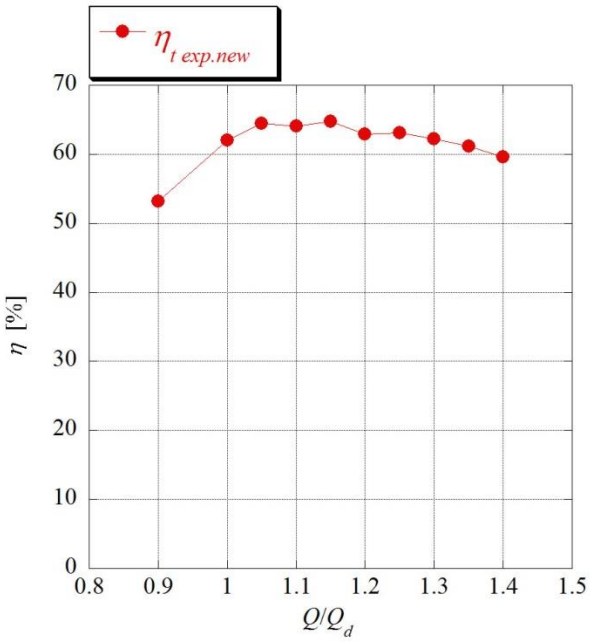

Figure 5-15 The new efficiency characteristic

In Figure 5-13, Figure 5-14, Figure 5-15, the experimental performance of the new model is clarified.

From the experimental result, we can find that the experimental result of the new model is similar to with numerical result of the new model. The power increases with the increasing of the flow rate. The head also increases with the increasing of the flow rate. The efficiency firstly increases with the flow rate. Then it reaches to the maximum, after that it decreases with the flow rate.

The comparison between experimental result of the new model and numerical result of the new model in the previous work is shown in Figure 5-16:

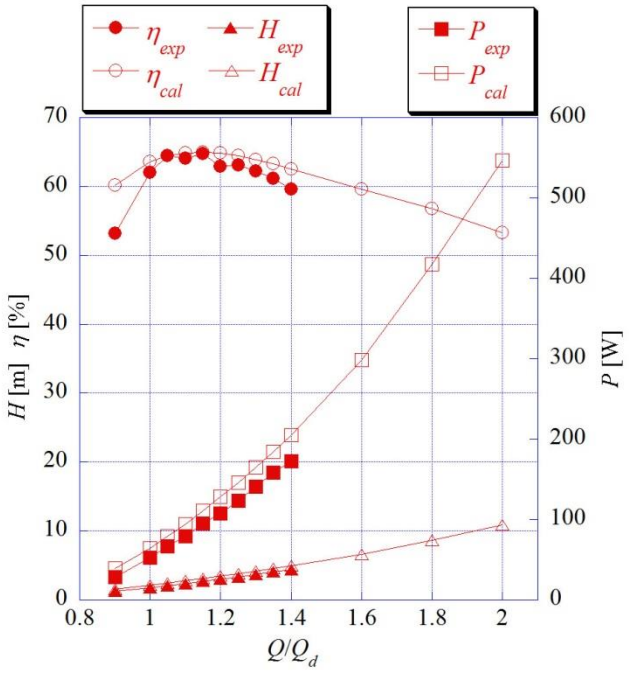

Figure 5-16 The comparison between experimental result and numerical result

The numerical result was compared with the experimental result, and they were well matched with each other.

Therefore, the numerical analysis of the new model is proved to be correct, and we can use this numerical model to make some prediction to the new model when we change some parameters of this small hydroturbine.

5.3 The simulation result of cylinder spoke

The performance comparison between cylinder spoke and cone spoke is shown in Figure 5-17.

From the performance curves we can see that compared with the cone spoke, the efficiency of test turbine with cylinder spoke increased in a wide flow rate range. The efficiency of test turbine firstly increased with the increasing of flow rate, then it reached to the highest point. After passing through the highest point it dropped down when the flow rate became larger. The maximum efficiency of test turbine with cylinder spoke reached to η_{max}=66.4% and it was obtained at 1.25Q_d. The maximum efficiency of test turbine with cone spoke was 64.2% at 1.2Q_d, therefore the efficiency of test turbine with cylinder spoke increased about 2.2%. However, the

efficiency at partial flow rate Q=0.9Q_d dropped as the same condition of cone spoke. Therefore, this is the own characteristic of the rotors, we can't improve it by changing the geometry of spokes. Compared with cone spoke, the head and power of test turbine with cylinder spoke didn't change much. Thus changing the geometry of spoke acts little effect on the head and power of the test turbine.

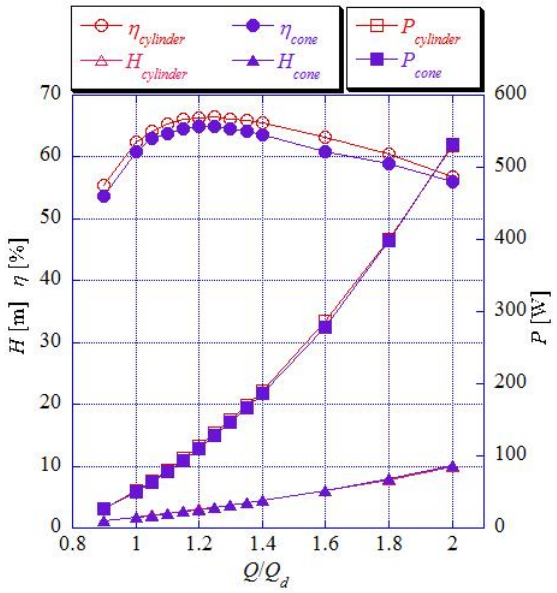

Figure 5-17 The performance comparison between cylinder spoke and cone spoke

In Figure 5-17, the horizontal axis is flow rate ratio between present flow rate Q and design flow rate Q_d. The first vertical axis is head and the efficiency of test turbine. The second vertical axis is the power of test turbine. The rotation speed is set to N_f=N_r=2300r/min.

The total pressure efficiency and the individual efficiency of front and rear rotor with cylinder spoke and cone spoke are curved in Figure 5-18, in order to clarify the detailed performance of each rotor.

The contra-rotating rotor is a kind of special structure, because there are two rotors compared with the traditional structure. Therefore, Figure 5-18 can help us to know the individual efficiency of front rotor and rear rotor, and this is very important for us to investigate the difference between this novel structure and the traditional structure.

According to the experience, the rear efficiency is the key point to enhance the total efficiency. Therefore, we should pay attention to the rear efficiency and the rear flow condition. Compared with the front efficiency and front flow condition, the rear efficiency and the rear flow condition have the wide changing range. Especially when the flow rate is smaller than the design flow rate, the rear efficiency is dramatically decreased. Therefore, we should observe the rear

efficiency carefully.

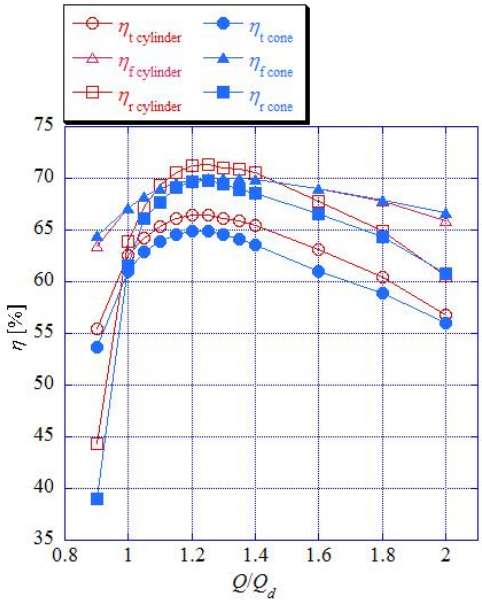

Figure 5-18 Total efficiency and individual efficiency of each rotor

Figure 5-18 shows that the performances of front rotor with two different spokes are almost the same with each other. That means changing the geometry of spokes acts little effect on the efficiency of front rotor. However, the efficiency of rear rotor under the condition of cylinder spoke increases in a wide range of flow rate.

The highest efficiency of rear rotor reached to 71.2% at $1.2Q_d$. Although the efficiency at partial flow rate $Q=0.9Q_d$ is still low, it increased about 5.3% compared with cone spoke, reaching to 44.4%. This will benefit the total efficiency of test turbine at partial flow rate, because it is this acute falling of rear efficiency that results in the large decreasing of total efficiency. The maximum of rear efficiency is even bigger than front efficiency under the condition of cylinder spoke. The increasing of rear efficiency means that the turbulent flow in front of rear blade was suppressed by the new spokes.

From Figure 5-18 we can observe that at large flow rate $Q=2.0Q_d$ the individual efficiency of front and rear rotor at cone spoke condition are higher than the individual efficiency of front and rear rotor at cylinder condition, while the total efficiency at cone condition is lower than the total efficiency at cylinder condition. The reason of this phenomenon is that the spoke efficiency of cylinder spoke is much higher than that of cone spoke.

The spoke efficiency of cone spoke and cylinder spoke are curved in Figure 5-19.

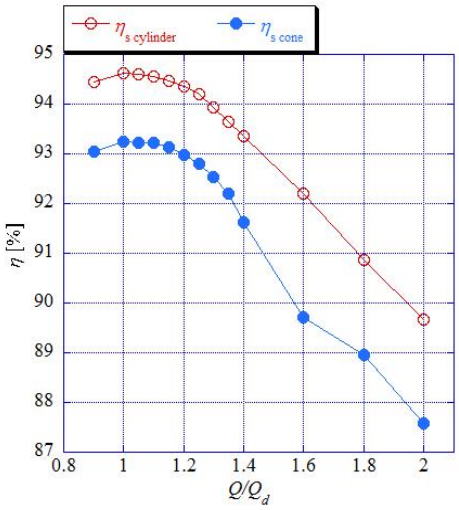

Figure 5-19 The spoke efficiency of cone spoke and cylinder spoke

At the flow rate Q=2.0Q_d the spoke efficiency of cylinder spoke is 89.7%, and that of cone spoke is 87.6%. The cylinder shape is 2.1% higher than the cone shape. The contra-rotating small hydro-turbine consists of three parts, including the front rotor, the spacer and the rear rotor. Thus we should consider the spoke efficiency when we calculate the total efficiency. At the condition of cone spoke, although the individual efficiency of front and rear rotor is 66.7% and 60.7% at Q=2.0Q_d, a little higher than that of cylinder spoke 65.9% and 60.5%, the spoke efficiency is much lower than that of cylinder spoke. This is why the individual efficiency of front and rear rotor at cone condition are higher than that of cylinder condition, but the total efficiency is lower.

From Figure 5-19 we can also observe that the spoke efficiency of cylinder shape is always higher than the efficiency of cone shape, and it is this cylinder shape help to enhance the spoke efficiency, and furthermore enhancing the total efficiency. However, the total efficiency at large flow rate Q=2.0Q_d just increased a little. That means the turbulent flow was not improved a lot and the internal flow condition deteriorated at very large flow rate condition. Thus we should avoid this small hydro-turbine working at very large flow rate condition to keep it high efficiency.

The internal flow condition between front rotor and rear rotor is quite important for this contra-rotating small hydro-turbine, and a good internal flow condition can make the small hydro-turbine perform higher efficiency. The spokes have blockage effect to the water, but we have to keep them there because they are the only supporting for the spacer and rotors. Thus the geometry of the spokes are changed to improve the internal flow condition.

The static pressure distributions between front rotor and rear rotor are shown in Figure 5-20 and Figure 5-21 respectively in the viewpoint of blade to blade.

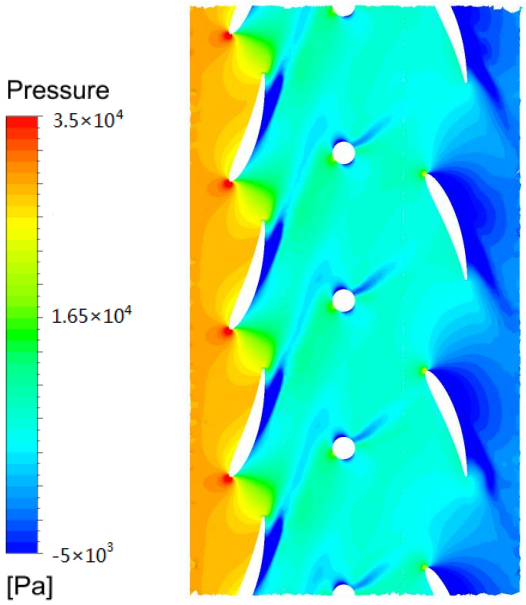

Figure 5-20 Static pressure distribution of cone spoke

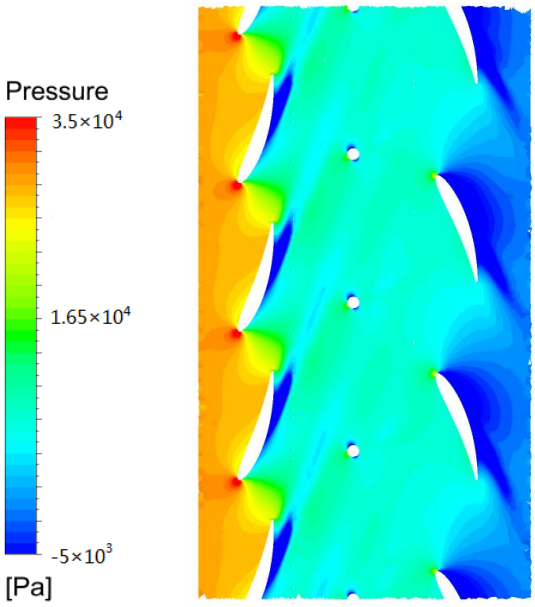

Figure 5-21 Static pressure distribution of cylinder spoke

Figure 5-20 is the cone spoke and Figure 5-21 is the cylinder spoke. The left side of the spoke is front rotor and the right side of the spoke is rear rotor. The flow rate is $1.2Q_d$ and the radial position is r/r_c=0.85, r represents the present radius and r_c represents the radius of the casing. The static pressure ranges from -5×10^3 Pa to 3.5×10^4 Pa.

The front rotor moves from up to down and the rotating direction of the rear rotor is from down to up. In order to judge the position of the rotors when they are rotating, we define two

angles θ_f and θ_r to describe the position of the front and rear blade. When we built the model of the blade, we used a base line to separate the blade into two parts, one part occupied 25% of the blade chord length and another part occupied 75% of the blade chord length. Then we chose this base line to define the meridian plane. Therefore, the front and rear blade were divided into two parts by the meridian plane, and we define this moment as the beginning position of rotating. When the rotor started to rotate, the base line of front blade and rear blade also deviated from the meridian plane and would have an angle with the meridian plane. Thus we define θ_f as the angle between base line of front blade and meridian plane, and θ_r as the angle between base line of rear blade and meridian plane.

Figure 5-20 and Figure 5-21 are at the beginning position of rotating. At this moment, we define θ_f =0 °and θ_r=0 °. That means the base line of front rotor and rear rotor are staying together with meridian plane. Each time step the rotor would rotate 3 °. Therefore, on the next time step θ_f =3 ° and θ_r=-3 °. There is a minus θ_r=-3 °, because the front and rear rotor are rotating in the contrary direction. We define the rotating direction of front rotor as the positive direction, then the rotating direction of rear rotor is negative. So we can use this method to describe the position of front and rear rotor when they are rotating.

From Figure 5-20 and Figure 5-21, we can see that the pressure behind the cone spoke is lower than that of cylinder spoke. That means the wake areas of cylinder spoke are smaller than that of cone spoke. The wake is the key factor which disturbs the flow direction and confuses the attack angle of rear blade. That is the reason why the wake areas become smaller will result in the increasing of the rear rotor efficiency.

5.4 The foreign vegetable materials experiment

The small hydroturbine is easy to be out of control when there are foreign vegetable materials in the fluid media. Therefore, we adopt the contra-rotating rotors to improve the running stability of the small hydroturbine. In order to clarify the running stability of the contra-rotating small hydroturbine, we make the foreign vegetable materials experiment.

The high speed camera (Phantom V310) is used during the visualization experiments to investigate the internal flow when there were foreign vegetable materials in the water. The imaging speed of this high speed camera is 5273fps, and we capture about 2 seconds when foreign materials flowed in front of test rotors. We also used the lighting source TROPICAL TL-500 made by LPL Ltd to supply for the quantity of light. Two kinds of foreign materials are chosen to conduct these experiments.

The small type was cudweed (15mm length, 7mm width), and the middle type is Philadelphia fleabane (55mm length, 15mm width). These two kinds of foreign vegetable materials are shown in Figure 5-22 and Figure 5-23 respectively, and a ruler is beside them to

illustrate their length.

Figure 5-22 The cudweeds used during the experiments

Figure 5-23 The Philadelphia fleabanes used during the experiments

The foreign vegetable materials were put into the tank upstream of the front and rear rotor. The leaves flowing through the front and rear rotor were counted and the experiments process, for example the attachment process of the leaves, were saved as animation to investigate.

During the first experiment, we respectively put 60 cudweeds into the water from the tank, and 34 of them flowed into the test section, then the animation about 2 seconds were saved to investigate the passing ratio. During the second experiment, 30 Philadelphia fleabanes were put into the tank respectively in several seconds and some of them flowed into the test section. By means of the same method, we investigated the passing ratio. These two kinds of leaves are grown in the middle of a year, we got these leaves at winter and conducted the experiments at the same time.

The result of this foreign vegetable materials experiment of cudweeds at the designing flow rate is shown in Table 5-1, including the ratio of the passing leaves which flow into the test section.

From Table 5-1, we can see that more than half (totally 34 cudweeds, 20 cudweeds were attached on the blades) of the 15mm length cudweeds were attached on the front and rear rotor. Among these attached leaves, 15 of 20 cudweeds were attached on the front rotor, another 5 cudweeds were attached on the rear rotor. Thus the attachment ratio of front rotor is much higher than that of rear rotor. We can also infer from Table 5-1 that the passing ratio of front rotor is 55.9%, and that of rear rotor is 73.7%.

Table 5-1 Experiment result of foreign vegetable materials

	Number of cudweeds	Passing rate
Number of cudweeds at inlet of front rotor	34	
Passing number in front rotor	19	19/34(55.9%)
Number of cudweed at inlet of rear rotor	19	
Passing number in rear rotor	14	14/19(73.7%)
Passing number in both front rotor and rear rotor	14	14/34(41.2%)

The result of visualization experiment when the cudweeds passed through the front rotor at the designing flow rate is shown in Figure 5-24.

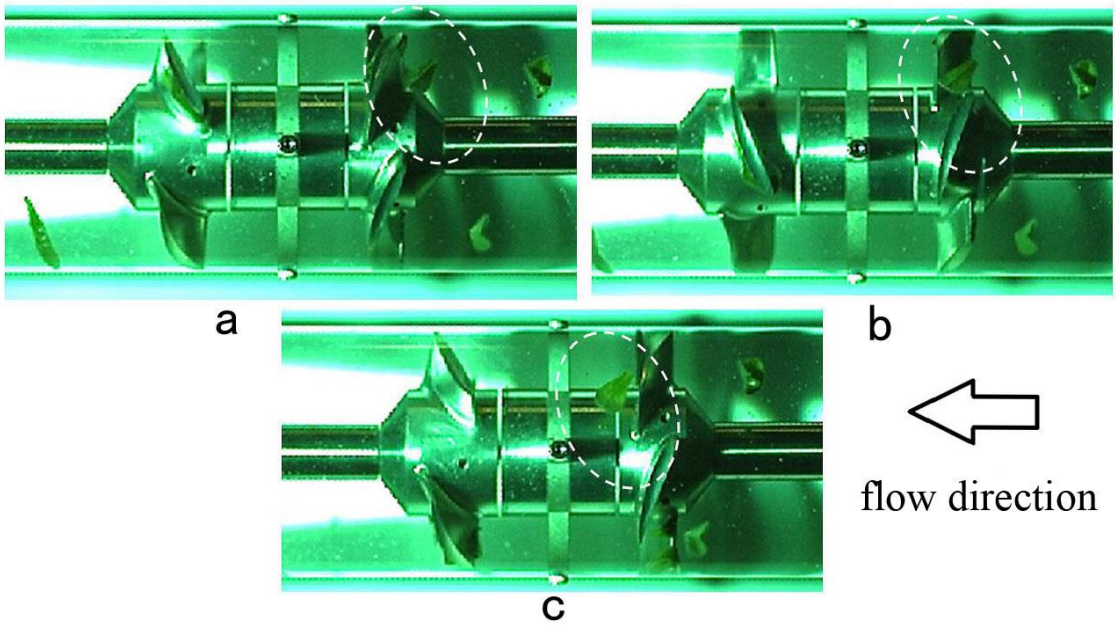

Figure 5-24 Visualization result when a piece of cudweed passed through the front rotor

Figure 5-24 (a), (b) and (c) illustrate 3 moments of the flowing process. Photo (a) is the moment when a piece of cudweed was right front of the leading edge of the front rotor, photo (b) is the moment when the cudweed was passing through the front rotor, photo (c) is the moment when the cudweed just passed through the front rotor.

From the passing process of a piece of cudweed, we can infer that the pitch is a significant parameter for the passing ability of this small hydro-turbine when there are foreign vegetable materials in the water. Therefore, we can reduce the number of blade to enlarge the pitch so that the passing ability will increase together. However, the following influence of the decreasing on performance when we reduce the number of blade has to be considered, either.

The result of visualization experiment when the cudweeds were attached on the leading edge of front rotor at the designing flow rate is shown in Figure 5-25.

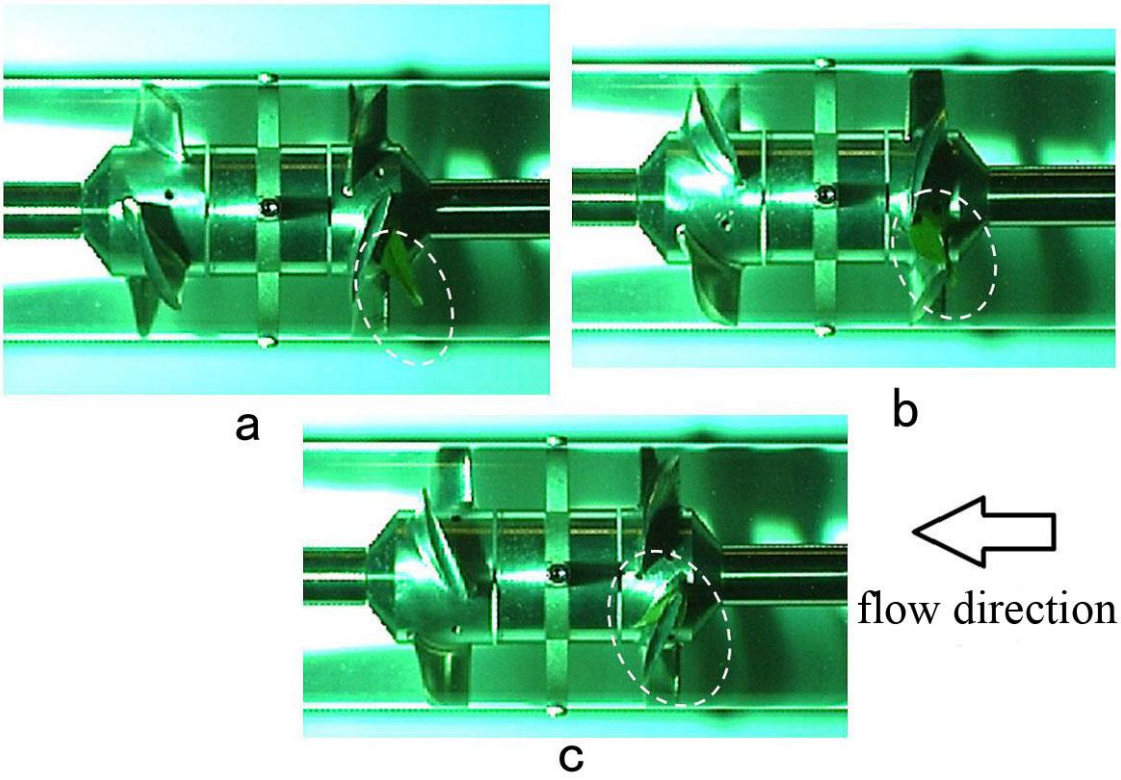

Figure 5-25 Visualization result of cudweed attached on the leading edge of front rotor

Figure 5-25 (a), (b) and (c) illustrate 3 moments of the attachment process. Photo (a) is the moment when a piece of cudweed was right front of the leading edge of front rotor, photo (b) is the moment when the cudweed was contacted with the leading edge of front rotor, photo (c) is the moment when the cudweed was just attached on the leading edge of front rotor.

From the photos we can see that at first the center of the cudweed contacted with the leading edge of front rotor, then the entire cudweed was folded and attached on the blade. The other 14 cudweeds were attached as the same way, thus the passing ability of leading edge is an important character to the small hydro-turbine. (However, some of the cudweeds which contacted with the leading edge also can pass through the rotor.) During the experiment, the attached cudweeds were folded and then rotated with the rotor under the condition of constant flow rate and rotation speed, they were not separated from the blade. The cudweeds attachment processes of front rotor and rear rotor were almost the same.

The result of visualization experiment when the Philadelphia fleabanes were attached on the leading edge of front rotor at the designing flow rate is shown in Figure 5-26.

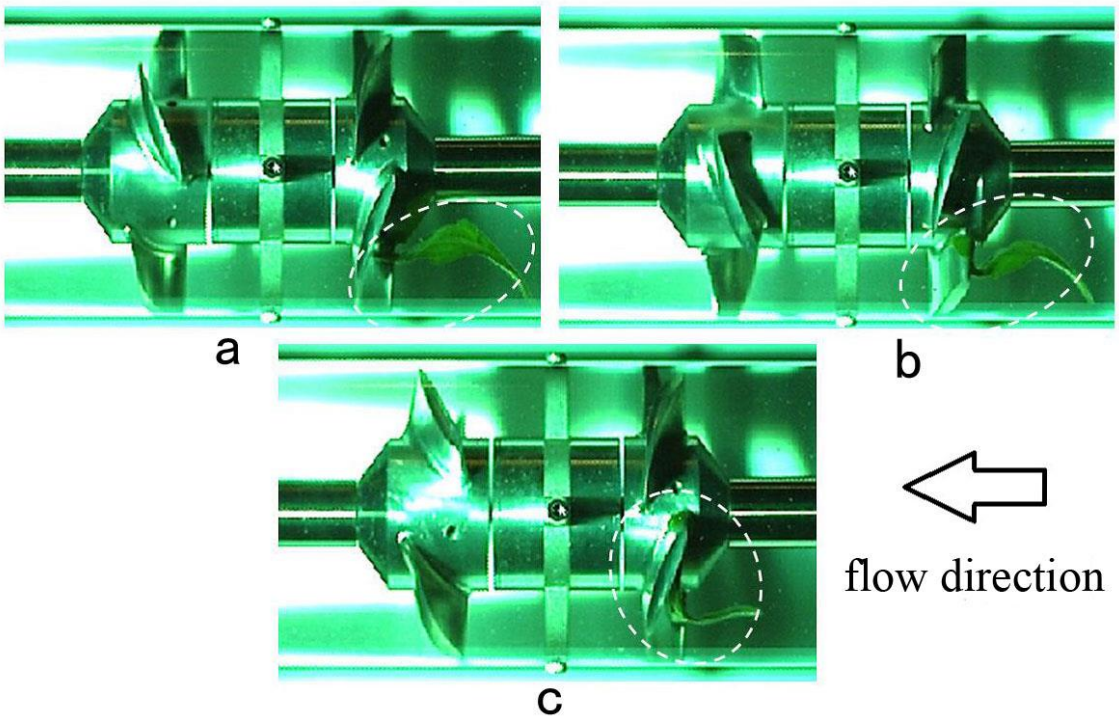

Figure 5-26 Visualization result of Philadelphia fleabane attached on the leading edge of front rotor

Figure 5-26 (a), (b) and (c) illustrate 3 moments of the attachment process. Photo (a) is the moment when a piece of Philadelphia fleabane was right front of the leading edge of front rotor, photo (b) is the moment when the Philadelphia fleabane was contacted with the leading edge of front rotor, photo (c) is the moment when the Philadelphia fleabane was just attached on the leading edge of front rotor.

During the Philadelphia fleabanes experiment, all of the leaves were attached on the front

rotor. Considering the same experiment conditions, for example the pitch of front rotor, the flow rate, the rotation speed and the contacting possibility of the leaves and rotors, we can infer that this kind of long leaf (55mm length) was certain to contact and attach on the leading edge of blade because of the length. That is the reason why all of the leaves were attached on the front rotor. Therefore, we should prevent this kind of long leaves from meeting the small hydro-turbine, or this leaves would attach on the rotors and disturb the running of the small hydro-turbine.

This small hydro-turbine is planned to be used into the pipe of agriculture water. Therefore, this kind of long leaves are not easy to appear into the casing. In case of appearing and resulting in the decreasing of the performance, a filter should be installed upstream of this small hydro-turbine. However, the filter will reduce the flow rate of the water, and performance of the small hydro-turbine will be changed when there is a filter upstream of it. Thus we should prefer to a filter which has a suitable scale hole on it to keep this small hydro-turbine perform normally. In the future, other kinds of foreign vegetable materials will be used in the experiments, and a suitable size of the filter hole which is installed upstream of the small hydro-turbine will be discussed and decided.

The foreign vegetable materials also have an effect on the performance of this contra-rotating small hydro-turbine, and the experiment was conducted to investigate this kind of effect. However, there are so many complicated situations when there are foreign vegetable materials in the water, and it is impossible to investigate them all.

Therefore, we choose a representative situation to investigate and we believe that this situation can reflect the effect of foreign vegetable materials on the performance of this contra-rotating small hydro-turbine. This representative situation is that two pieces of cudweeds are attached on the blade of front rotor. The photos of the performance experiment under this situation are shown on Figure 5-27 and Figure 5-28.

Figure 5-27 Performance experiment of attaching

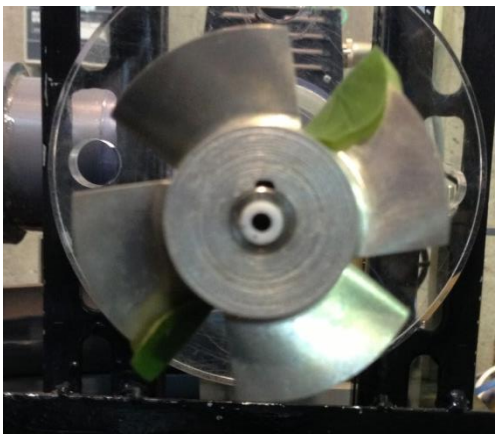

Figure 5-28 Another view of experiment

The maximum flow rate of the experiment was $1.4Q_d$ because of the limitation of measurement instruments. In this research, to investigate the stability of this contra-rotating small hydro-turbine, we conducted performance experiment when two pieces of cudweeds were attached on the blade of front rotor. The comparison between the performance without foreign vegetable materials and the performance when two pieces of cudweeds were attached on the blade of front rotor is shown on Figure 5-29.

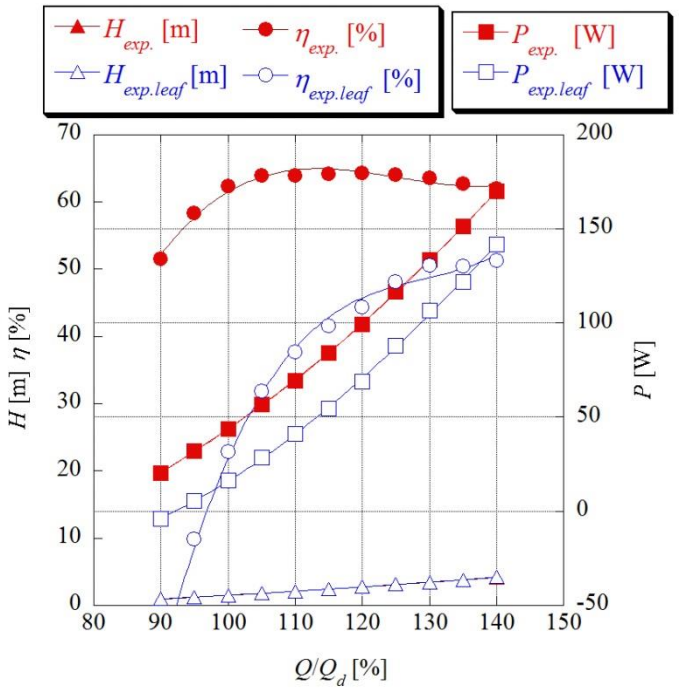

Figure 5-29 Comparison between cudweeds and without cudweeds

From Figure 5-29, we can see that it is hard to distinguish the difference of the head, they are almost same in the Figure 5-29. Therefore, the foreign vegetable materials have little effect on the head of the contra-rotating small hydro-turbine. However, the efficiency and power have obvious changing during the performance experiment, especially for the efficiency.

For the power, it almost has an equal decreasing at each measurement point of flow rate, and the change tendency of these two situations is almost the same. That means the effect of foreign vegetable materials on the power is uniform at each point of flow rate, the effect on power will not change with the changing of flow rate. At the designing flow rate, the power without the foreign vegetable materials is P=43.8W, and the power with the foreign vegetable materials is P=16.2W. Therefore the foreign vegetable materials bring about 27.6W decreasing of the power.

For the efficiency, it has a changing difference at different points of flow rate. At partial flow rate, it has the larger decreasing, and the efficiency can be even down to 0% near the flow

rate of Q=0.9Q_d. That means when this contra-rotating small hydro-turbine was attached on the foreign vegetable materials at partial flow rate, it will lose the ability of generating electricity. Therefore, we should not let this contra-rotating small hydro-turbine operate at partial flow rate. The highest efficiency has also decreased because of the foreign vegetable materials. The highest efficiency when there are not foreign vegetable materials in the water is η=64.2%, and it is obtained at 1.2Q_d. The highest efficiency when two pieces of cudweeds are attached on the blade of front rotor is η=51.2%, and it is obtained at 1.4Q_d. Therefore, the foreign vegetable materials bring about 13% decreasing of highest efficiency, and they make the highest efficiency move to the flow rate of Q=1.4Q_d.

CHAPTER 6

CONCLUSIONS

The geometry of the spoke was changed from cone to cylinder, and the numerical simulation was conducted under the condition of these two different kinds of spoke. The effect of cylinder spoke to the performance and internal flow condition of this contra-rotating small hydro-turbine was clarified by the numerical analysis.

Besides, the visualization experiments with cudweeds and Philadelphia fleabanes, which can help to make clarified the internal flow condition and passing ability when there are foreign vegetable materials in the water, are conducted. We choose the cudweed as the small type foreign vegetable materials and the Philadelphia fleabane as the middle type foreign materials. To investigate the effect of foreign vegetable materials on the performance of this contra-rotating small hydro-turbine, the performance experiment under the situation that two pieces of cudweeds are attached on the blade of front rotor is also conducted.

According to the experiment results and numerical results, we can make the following conclusions:

(1) The efficiency of this contra-rotating small hydro-turbine has a falling at partial flow rate Q=0.9Q_d regardless of the geometry changing of spokes. The cylinder spoke are not able to stop the falling of efficiency at partial flow rate. It is the own characteristic of front rotor and rear rotor. Therefore, in order to keep it high efficiency, this contra-rotating small hydro-turbine should not be operated at partial flow rate.

(2) Compared with the test turbine under cone spoke condition, the efficiency of test turbine with cylinder rotor increased in a wide range of flow rate. The highest efficiency of the test turbine with cylinder spoke increased about 2.2%, reaching to 66.4%, and it was obtained at 1.25Q_d. The spoke efficiency increasing contributes to the enhancing of total efficiency at cylinder condition. However, the efficiency just increased a little at very large flow Q=2.0Q_d. Thus changing the spoke geometry has little benefit for the efficiency increasing at very large flow rate.

(3) The cylinder spokes can suppress the wake areas behind the spokes themselves and make the pressure of these areas stable and closed to the nearby areas. This is quite useful for increasing the efficiency of rear rotor because smaller wake areas could improve the flow condition in front of the rear rotor. The total efficiency of this small hydro-turbine will make a progress when the rear efficiency and spoke efficiency are increased and internal flow conditions are improved.

(4) The passing rate of cudweed is 41.2%, and all of the Philadelphia fleabane can’t pass

through this contra-rotating small hydro-turbine. The leading edge of blade is easier to be attached with the foreign vegetable materials. We can decrease the number of blade or use the low-solidity blade to improve the passing ability, however, we have to consider the drop of performance at the same time.

(5) The effect of foreign vegetable materials on the performance of this contra-rotating small hydro-turbine is investigated when two pieces of cudweeds are attached on the blade of front rotor. The power almost has an equal decreasing which value is about 27.6W at the measurement points of flow rate. The highest efficiency under the situation that two pieces of cudweeds are attached on the blade of front rotor is 51.2%, and it is obtained at $1.4Q_d$. The foreign vegetable materials bring about 13% decreasing of the highest efficiency, and make the highest efficiency move to the flow rate of $Q=1.4Q_d$.

(6) This small hydro-turbine is planned to be used into the pipe of agricultural water. To protect the long foreign vegetable materials attaching on the leading edge of blade, a filter should be installed upstream of this contra-rotating small hydro-turbine, and the size of the filter hole should be discussed and decided.

ACKNOWLEDGEMENT

This research was supported by Adaptable and Seamless Technology Transfer Program (NO. AS262Z00175L) through Targetdriven R&D from JST, JKA and its promotion funds from KEIRIN RACE (NO. 27-176 and NO. 28-125), the Awa Bank Science and Culture Foundation, the Grant-in-Aid for Young Scientists (B) from Japan Society for the Promotion of Science No.24760138, No.16K18017, TEPCO Memorial Foundation and Hatakeyama Culture Foundation. We would like to show our special thanks for the foundations.

In the end of this graduation thesis, I want to show my feeling of gratitude to Professor Toru Shigemitsu. Professor Toru Shigemitsu is an excellent teacher. He points out the research direction for me and helps me to carry out my research project. Besides, he also supports me to take part in the international conferences. Taking part in these international conferences helps me to expand my horizon and gives me chances to communicate with other researchers in my research field. I benefit a lot from my research project and the international conferences. Thanks again for the help of Professor Toru Shigemitsu.

Some students have also helped me to finish my experiments, and I also want to show my feeling of gratitude to them. They are:

Yasutoshi Takeshima

Tomofumi Ikebuchi

Thanks for their help and wish them all the best.

At last, thanks for the professors who review my graduation thesis, and thanks for the professors who take part in my graduation presentation. Thanks for your suggestions concerning my graduation thesis.

REFERENCES

1. 古川 明徳・他 3 名, ダリウス形水車による低落差水力の有効利用に関する一考察, 日本機械学会論文集(B 編), 64-624(1998), 2534-2540.
2. 金元 敏明・他 3 名, 極浅水流を有効利用するジャイロ形水車の開発(第 1 報 : ランナの作動原理と水車運転の実証), 日本機械学会論文集(B 編), 70-690,(2004), 413-418.
3. 松井 純, らせん水車の内部流れと性能, ターボ機械, 38-6(2010), 358-364.
4. Toshihiko I., Shouichiro I and Kenji T., Performance of nano-hydraulic turbine utilizing waterfalls, Renewable Energy, 35 (2010), 293-300.
5. Nakajima M., Shouichiro I and Toshihiko I., Performance of Savonius Rotor for Environmentally Friendly Hydraulic Turbine, JFST, 3-3(2008), 420-429.
6. 飯尾 昭一郎・他 3 名, 遮へい板を利用した環境融和型サボニウス水車の効率改善, ターボ機械, 37-12(2009), 743-748.
7. 飯尾 昭一郎・他 3 名, 環境融和型ナノ水車発電機の実証実験における不具合事例, ターボ機械, 39-3(2011), 162-168.
8. 水力機械工学便覧編集委員会, 水力機械工学便覧, コロナ社, 昭和 35 年再版
9. 佐野 新三郎・有江 幹男, 新版 水力学および水力機械, 工学図書, 昭和 37 年初版
10. 今木 清康, 流体機械工学, コロナ社
11. 辻 茂, 大学基礎流体機械, 実教出版
12. 妹尾泰利, 内部流れ学と流体機械, 株式会社養賢堂
13. 大橋秀雄, 流体力学（1), コロナ社, 新日本印刷株式会社
14. 小林大作, ターボ機械協会　ターボ機械－入門編－〔新改訂版〕, 日本工業出版株式会社
15. 今市憲作 他 2 名, ポンプ設計の基礎, 日本工業出版, 昭和 58 年 初版
16. Nan D, Shigemitsu T, Zhao SD, Ikebuchi T, Takeshima Y. Study on performance of contra-rotating small hydro-turbine with thinner blade and longer front hub, Renewable Energy, 117(2018), 184-192.
17. Nan D, Shigemitsu T, Zhao SD and Takeshima Y. Numerical analysis of contra-rotating small hydro-turbine with cylinder spoke. International Journal of Fluid Machinery and Systems, 11(2018), 21-29.
18. Nan D, Shigemitsu T, Zhao SD and Takeshima Y. Internal flow and performance with foreign vegetable materials in a contra-rotating small hydro-turbine. International Journal of Fluid Machinery and Systems, 10(2017), 385-393.